Metric-Based Upscaling

HOUMAN OWHADI
California Institute of Technology

AND

LEI ZHANG
California Institute of Technology

Abstract

We consider divergence form elliptic operators in dimension $n \geq 2$ with L^∞ coefficients. Although solutions of these operators are only Hölder-continuous, we show that they are differentiable ($C^{1,\alpha}$) with respect to harmonic coordinates. It follows that numerical homogenization can be extended to situations where the medium has no ergodicity at small scales and is characterized by a continuum of scales. This new numerical homogenization method is based on the transfer of a new metric in addition to traditional averaged (homogenized) quantities from subgrid scales into computational scales. Error bounds can be given and this method can also be used as a compression tool for differential operators.

1 Introduction and Main Results

Let Ω be a bounded and convex domain of class C^2. We consider the benchmark PDE

$$\begin{cases} -\operatorname{div}(a(x)\nabla u(x)) = g & \text{in } \Omega \\ u = 0 & \text{in } \partial\Omega \end{cases} \tag{1.1}$$

where g is a function in $L^\infty(\Omega)$ and $x \to a(x)$ is a mapping from Ω into the space of positive definite symmetric matrices. We assume a to be symmetric and uniformly elliptic with entries in $L^\infty(\Omega)$.

- Is it possible to upscale (1.1)?

Homogenization theory [15, 54] allows us to do so by transferring bulk (averaged) information from subgrid scales into computational scales. This transfer from a numerical homogenization point of view is justified under two fundamental assumptions:

- ergodicity at small scales and
- scale separation.

Can we get rid of these assumptions?

Communications on Pure and Applied Mathematics, Vol. LX, 0675–0723 (2007)

- Can we numerically homogenize (1.1) when a is arbitrary? In particular, can we when a is characterized by a continuum of scales with no ergodicity at small scales?

What do we mean by numerical homogenization when a is arbitrary? It is important to recall that F. Murat and L. Tartar's theory of H-convergence [61] provides a mathematical framework for analysis of composites in complete generality without any need for geometrical hypotheses such as periodicity or randomness. This theory is based on a powerful tool called compensated compactness or the div-curl lemma introduced in the 1970s by Murat and Tartar [60, 73], which has been characterized by a wide range of applications and refinements [26]. Here we consider homogenization from a slightly different point of view: we want to solve (1.1) on a coarse mesh, and we want to understand which information should be transferred from fine scales to coarse scales when the entries of a are arbitrary. For that purpose we need a new form of compensation given in Section 1.1.

It is important to observe that if one needs to solve (1.1) only one time (with one g) the method proposed here does not reduce the number of numerical operations.[1] Indeed, we need to compute (1.1) n times (n being the space dimension) with 0 in the right-hand side in (1.1) and linear boundary conditions. However, if one needs to solve (1.1) for a large number (M) of different right-hand sides g ($M \gg n$, which would happen if one tries to optimize specific properties of u with respect to g) then the methods proposed here have a practical use since they basically say that after solving (1.1) n times it is sufficient to solve (1.1) on a coarse mesh (with $N^{0.01}$ nodes instead of N, for instance) M times.

Let us recall that (1.1) can be solved in $O(N(\ln N)^{n+3})$ operations using hierarchical matrix methods [9, 10, 11, 12, 13] or in $O(N)$ operations using iterative methods (see [76, 77]).

Finally, the point of view of this paper is to observe the "redundancy" of solutions of (1.1) at small scales rather than "fast computation." Indeed, it is not obvious that (1.1) can be homogenized when the medium does not satisfy the usual assumptions on periodicity, ergodicity, or scale separation. Moreover, if (1.1) can indeed be homogenized, it is important to understand what minimal quantity of information should be kept from small scales to obtain an accurate homogenized operator. Once the correct coarse parameters are identified (the bulk quantities and the upscaled metric), one can try to model, estimate, or simulate them, but the first step is to identify them.

1.1 A New Form of Compensation

To introduce the new form of compensation, we need to introduce the so-called a-harmonic coordinates associated to (1.1), i.e., the weak solution of the boundary

[1] It will be shown in [67] that for parabolic and reaction-diffusion equations the situation is different: the methodology introduced in this paper can be used to reduce the number of operations even when one needs to solve these equations only once.

value problem

$$\begin{cases} \operatorname{div} a\nabla F = 0 & \text{in } \Omega \\ F(x) = x & \text{on } \partial\Omega. \end{cases} \tag{1.2}$$

By (1.2) we mean that F is an n-dimensional vector field $F(x) = (F_1(x), \ldots, F_n(x))$ such that each of its entries satisfies

$$\begin{cases} \operatorname{div} a\nabla F_i = 0 & \text{in } \Omega \\ F_i(x) = x_i & \text{on } \partial\Omega. \end{cases} \tag{1.3}$$

The new compensation phenomenon is controlled by the following object:

DEFINITION 1.1 We write

$$\sigma := {}^{\mathsf{T}}\nabla F a \nabla F. \tag{1.4}$$

We write μ_σ for the anisotropic distortion of σ defined by

$$\mu_\sigma := \operatorname{ess\,sup}_{x\in\Omega}\left(\frac{\lambda_{\max}(\sigma(x))}{\lambda_{\min}(\sigma(x))}\right) \tag{1.5}$$

where $\lambda_{\max}(M)$ and $\lambda_{\min}(M)$ denote the maximal and minimal eigenvalues of M, respectively.

DEFINITION 1.2 In dimension $n = 2$, we say that σ is *stable* if and only if $\mu_\sigma < \infty$ and there exists a constant $\epsilon > 0$ such that $(\operatorname{tr}(\sigma))^{-1-\epsilon} \in L^1(\Omega)$.

Remark 1.3. According to [4], in dimension 2 if a is smooth then σ is stable. According to [1], F is always an homeomorphism in dimension 2 even with $a_{i,j} \in L^\infty(\Omega)$.

THEOREM 1.4 *Assume that σ is stable and $n = 2$. Then there exist constants $\alpha > 0$ and $C > 0$ such that $(\nabla F)^{-1}\nabla u \in C^\alpha(\Omega)$ and*

$$\|(\nabla F)^{-1}\nabla u\|_{C^\alpha(\Omega)} \le C\|g\|_{L^\infty(\Omega)}. \tag{1.6}$$

Remark 1.5. The constant α depends on Ω, $\lambda_{\max}(a)/\lambda_{\min}(a)$, and μ_σ. The constant C depends on the constants above, $\lambda_{\min}(a)$, and $\|(\operatorname{tr}(\sigma))^{-1-\epsilon}\|_{L^1(\Omega)}$. We use the notation $\lambda_{\max}(a) := \sup_{x\in\Omega}\sup_{|\xi|=1} {}^{\mathsf{T}}\xi a\xi$ and $\lambda_{\max}(a) := \inf_{x\in\Omega}\inf_{|\xi|=1} {}^{\mathsf{T}}\xi a\xi$.

Remark 1.6. If one considers a sequence a_ϵ such that μ_{σ_ϵ} and $\|(\operatorname{tr}(\sigma_\epsilon))^{-1-\epsilon}\|_{L^1(\Omega)}$ are uniformly bounded away from ∞ and $\lambda_{\min}(a_\epsilon)$ and $\lambda_{\max}(a_\epsilon)$ are uniformly bounded away from 0 and ∞, then (1.6) is uniformly true. If we consider a periodically oscillating sequence $a_\epsilon(x) = a(x/\epsilon)$, $\mu_{\sigma_1} < \infty$, and $\|(\operatorname{tr}(\sigma_1))^{-1-\epsilon}\|_{L^1(\Omega)} < \infty$, then (1.6) is uniformly true.

Remark 1.7. It is easy to check from the proofs of Theorem 1.4 and Theorem 2.4 that if $(\operatorname{tr}(\sigma_\epsilon))^{-1} \in L^q(\Omega)$ (with $q > 2$), then it is possible to replace $\|g\|_{L^\infty(\Omega)}$ by $\|g\|_{L^p(\Omega)}$ in (1.6) with p depending on q. More precisely, if $(\operatorname{tr}(\sigma_\epsilon))^{-1} \in L^\infty(\Omega)$, then it is possible to replace $\|g\|_{L^\infty(\Omega)}$ by $\|g\|_{L^{2+\epsilon}(\Omega)}$ in (1.6) for any $\epsilon > 0$.

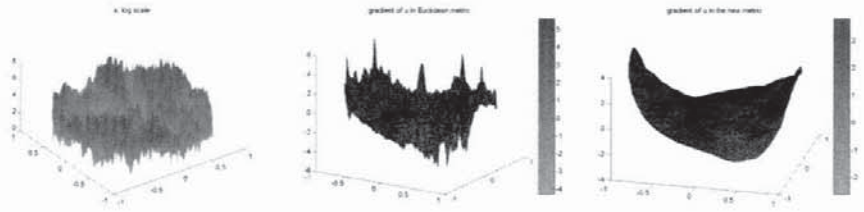

(a) a in log scale. **(b)** ∇u. **(c)** $(\nabla F)^{-1}\nabla u$.

FIGURE 1.1. Change of metric on the disk.

Remark 1.8. We don't need a to be symmetric to obtain 1.4, but for the clarity of the presentation we have chosen to restrict ourselves to that case. We have not analyzed Neumann boundary conditions; this will done in a later work.

Remark 1.9. We will use the notation $\nabla_F u := (\nabla F)^{-1}\nabla u$. In dimension 2, it is known [1, 4, 6] that the determinant of ∇F is strictly positive almost everywhere and the object $\nabla_F u$ is well-defined. In dimension 3 and higher $\nabla_F u$ is well-defined when σ is stable.

This phenomenon can be observed numerically. In Figures 1.1(a) and 1.2(a) a is given by a product of random functions oscillating over a continuum of scales. The entries of the matrix ∇F are in L^p (Figure 1.2(b)), the entries of the gradient of u in the Euclidean metric are in L^p (Figures 1.1(b) and 1.2(c)), yet $(\nabla F)^{-1}\nabla u$ is Hölder-continuous (Figures 1.1(c) and 1.2(d)).

Let us now introduce the compensation phenomenon in dimension $n \geq 3$. We call β_σ the Cordes parameter associated to σ defined by

$$\beta_\sigma := \operatorname{ess\,sup}_{x\in\Omega}\left(n - \frac{(\operatorname{tr}[\sigma(x)])^2}{\operatorname{tr}[{}^{\mathsf{T}}\sigma(x)\sigma(x)]}\right). \tag{1.7}$$

Observe that since β_σ is also given by

$$\beta_\sigma = \operatorname{ess\,sup}_{x\in\Omega}\left(n - \frac{(\sum_{i=1}^n \lambda_{i,\sigma(x)})^2}{\sum_{i=1}^n \lambda_{i,\sigma(x)}^2}\right), \tag{1.8}$$

where $(\lambda_{i,M})$ denotes the eigenvalues of M, it is a measure of the anisotropy of σ.

DEFINITION 1.10 In dimension $n \geq 3$, we say that σ is *stable* if and only if $\beta_\sigma < 1$ and, if $n \leq 4$, that there exists a constant $\epsilon > 0$ such that $(\operatorname{tr}(\sigma))^{n/2-2-\epsilon} \in L^1(\Omega)$.

Remark 1.11. According to [4, 21] in dimension 3 and higher σ can be unstable even if a is smooth. We refer to Figure 1.6 for an explicit example.

Let us write

$$\|v\|_{W_0^{2,p}(\Omega)} := \left(\int_\Omega \left(\sum_{i,j=1}^n |\partial_i\partial_j v|^2\right)^{p/2} dx\right)^{1/p}. \tag{1.9}$$

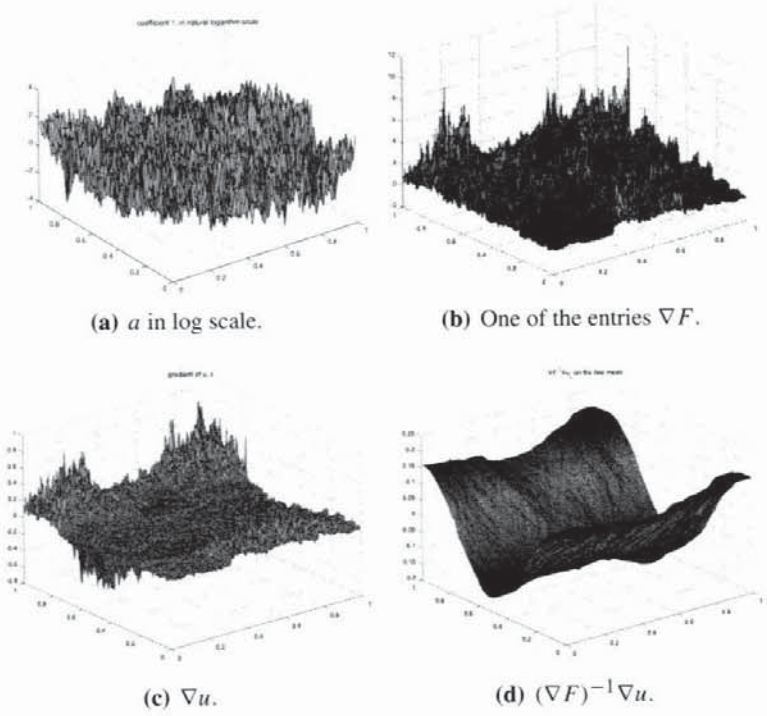

(a) a in log scale. **(b)** One of the entries ∇F.

(c) ∇u. **(d)** $(\nabla F)^{-1}\nabla u$.

FIGURE 1.2. Change of metric on the torus.

THEOREM 1.12 *Assume that σ is stable and $n \geq 3$. Then F is an automorphism on Ω. Moreover, there exist constants $p > 2$ and $C > 0$ such that $u \circ F^{-1} \in W_0^{2,p}(\Omega)$ and*

$$\|u \circ F^{-1}\|_{W_0^{2,p}(\Omega)} \leq C\|g\|_{L^\infty(\Omega)}. \tag{1.10}$$

Remark 1.13. The constant p depends on n, Ω, and β_σ. The constant C depends on the constants above, $\lambda_{\min}(a)$, and, if $n \leq 4$, on $\|(\mathrm{tr}(\sigma))^{n/2-2-\epsilon}\|_{L^1(\Omega)}$.

In the following theorem we do not need to assume that Ω is convex.

THEOREM 1.14 *Assume $n \geq 2$ and $(\mathrm{tr}(\sigma))^{-1} \in L^\infty(\Omega)$. Let $p > 2$. There exists a constant $C^* = C^*(n, \partial\Omega) > 0$ such that if $\beta_\sigma < C^*$ then there exists a real number $\gamma > 0$ depending only on n, Ω, and p such that*

$$\|(\nabla F)^{-1}\nabla u\|^2_{C^\gamma(\Omega)}\, dt \leq C\|g\|^2_{L^p(\Omega)}. \tag{1.11}$$

Remark 1.15. The constant C in (1.11) depends on n, γ, Ω, C^*, $\lambda_{\min}(a)$, $\|a\|_{L^\infty(\Omega)}$, μ_σ, and $\|(\mathrm{tr}(\sigma))^{-1}\|_{L^\infty(\Omega_T)}$.

1.2 Dimensionality Reduction

Observe that (1.1) is a priori an infinite-dimensional problem since a and g can be irregular at all scales. Yet according to Theorems 1.4 and 1.12, whatever the

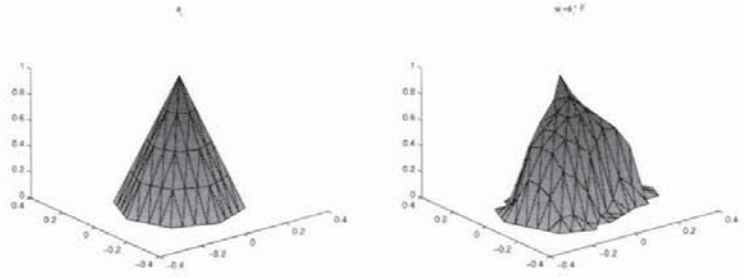

(a) φ_i. **(b)** $\psi_i = \varphi_i \circ F$.

FIGURE 1.3. The Galerkin elements.

choice of g, at small scales, solutions to (1.1) are correlated to F, which lives in a functional space of dimension n. More precisely, we will propose a rigorous justification of a variation of the multiscale finite element method[2] introduced by Hou and Wu [50] in its form refined by Allaire and Brizzi [2] in situations where the medium is not assumed to be periodic or ergodic (these methods are already rigorously justified when the medium is periodic [2, 50]).

Let $\mathcal{T}_h$ be a coarse conformal mesh on Ω composed of n-simplices (triangles in dimension 2 and tetrahedra in dimension 3). Here h is the usual resolution of the mesh defined as the maximal length of the edges of the tessellation. Let us call $\gamma(\mathcal{T}_h)$ the maximum over of the n-simplices K of $\mathcal{T}_h$ of the ratio between the radius of the smallest ball containing K and the largest ball inscribed in K. We assume $\gamma(\mathcal{T}_h)$ to be uniformly bounded in h.

We write $V_h \subset H^1(\Omega)$ the set of piecewise linear functions on the coarse mesh vanishing at the boundary of the tessellation. We write $\mathcal{N}_h$ the set of interior nodes of the tessellation and φ_i ($i \in \mathcal{N}_h$) the usual nodal basis function of V_h satisfying

$$\varphi_i(y_j) = \delta_{ij}. \tag{1.12}$$

We consider the elements $(\psi_i)_{i\in\mathcal{N}_h}$ defined by

$$\psi_i := \varphi_i \circ F(x). \tag{1.13}$$

Let us write u_h the solution of the Galerkin scheme associated to (1.2) based on the elements $(\psi_i)_{i\in\mathcal{N}_h}$. Observe that the number of elements is on the order of h^{-n} and we have the following theorem:

THEOREM 1.16 *Assume that σ is stable and $n = 2$. Then there exist constants $\alpha, C > 0$ such that*

$$\|u - u_h\|_{H^1} \leq Ch^{\alpha}\|g\|_{L^{\infty}(\Omega)}. \tag{1.14}$$

[2] Let us recall that the multiscale finite element method is inspired from Tartar's oscillating test functions [74].

Remark 1.17. The constant α depends only on n, Ω, and μ_σ. The constant C depends on the objects mentioned above plus $\|(\mathrm{tr}(\sigma))^{-1-\epsilon}\|_{L^1(\Omega)}$, $\lambda_{\min}(a)$, $\lambda_{\max}(a)$, and $\gamma(\mathcal{T}_h)$.

Remark 1.18. Theorem 1.16 is also valid with $\alpha = 1$ as in Theorem 1.23. The only difference between these two theorems lies in the constant C. In the proof of Theorem 1.16 we use the property $u \circ F^{-1} \in C^{1,\alpha}(\Omega)$, and in the proof of Theorem 1.23 we use the property $u \circ F^{-1} \in W^{2,2}(\Omega)$.

Remark 1.19. Let us recall that u_h is an element of the space X_h spanned by $(\psi_i)_{i\in\mathcal{N}_h}$ obtained as the solution of the linear problem

$$a[\psi_i, u_h] = (\psi_i, g)_{L^2(\Omega)} \tag{1.15}$$

where $a[\,\cdot\,,\cdot\,]$ is the bilinear form on $H_0^1(\Omega)$ defined by

$$a[v, w] := \int_\Omega \nabla v a \nabla w. \tag{1.16}$$

It follows from Theorem 1.16 that solutions to (1.1) live in the H^1-norm neighborhood of a low-dimensional space.

Remark 1.20. The proof of Theorem 1.16 is done for the exact function ψ_i and not for its discrete version on a fine mesh. If a is regular at a given small scale h_0, then it is easy to check that Theorem 1.16 remains valid as long as the edges of the fine mesh are smaller than h_0. A more intriguing case is when a is discrete and discontinuous on a fine mesh. Numerical experiments show that theorems such as 1.16 and 1.4 remain valid, but to justify them for the discrete version of the harmonic coordinates F and elements ψ_i one would have to adapt our theorems to the discrete setting. In order to remain concise, we have chosen not to include that adaptation in this paper.

Remark 1.21. We keep the composition rule used in [2]. The only difference between the elements (1.13) and the ones proposed by Hou, Wu, Allaire, and Brizzi lies in the fact that we use the global solution to (1.2) and not a local one computed on each triangle of the coarse mesh through an oversampling technique. We refer to Remark 3.1 for further comments.

Remark 1.22. Let S be the stiffness matrix $a[\psi_i, \psi_j]$. Then S^{-1} is in general dense (characterized by N^2 entries where N is the number of nodes of the mesh). Yet surprisingly, by combining Theorem 1.16 with theorem 5.4 of [13], one can approximate S^{-1} (in the L^2-norm) with hierarchical matrix M_H such that the matrix vector product by M_H requires only $O(N(\ln N)^{n+3})$ operations.

In dimension $n \geq 3$ we have the following estimate:

THEOREM 1.23 *Assume that σ is stable, $n \geq 3$, and $\|(\mathrm{tr}(\sigma))^{-1}\|_{L^\infty(\Omega)} < \infty$. Then there exist constants $\alpha, C > 0$ such that*

$$\|u - u_h\|_{H^1} \leq Ch\|g\|_{L^\infty(\Omega)}. \tag{1.17}$$

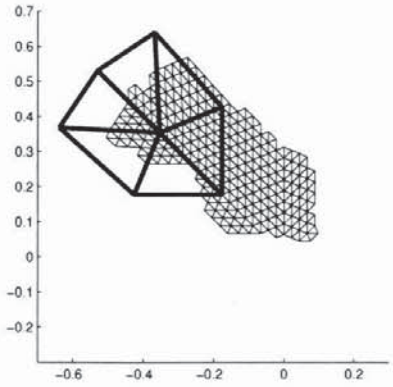

FIGURE 1.4. Support of the elements φ_i and ψ_i.

Remark 1.24. The constant C depends on n, $\gamma(\mathcal{T}_h)$, Ω, β_σ, $\lambda_{\max}(a)$, $\lambda_{\min}(a)$, and $\|(\mathrm{tr}(\sigma))^{-1}\|_{L^\infty(\Omega)}$.

1.3 Galerkin with Localized Elements

For clarity we will restrict ourselves from now on to dimension 2; the generalization of the statements to higher dimensions is conditioned on the stability of σ (and the application of Theorem 1.14).

The elements (1.13) can be highly distorted and nonlocal (Figure 1.4) since

$$\mathrm{supp}(\psi_i) := F^{-1}(\mathrm{supp}(\varphi_i)). \tag{1.18}$$

It follows that the elements ψ_i are piecewise linear on a fine mesh different from the one on which a is defined and F has been computed. Is it possible to avoid that difficulty by solving (1.1) on a coarse mesh with localized elements? The answer is yes, but the price to pay for the localization will be the discontinuity of the elements and the fact that the accuracy of the method will depend on a weak aspect ratio of the triangles of the tessellation in the metric induced by F.

More precisely, consider a triangle K of the tessellation, and call a, b, and c the nodes of K and θ the interior angle of the triangle $(F(a), F(b), F(c))$ that is the closest to $\pi/2$. We call the weak aspect ratio of the triangle K in the metric induced by F the quantity

$$\eta^F_{\min}(K) := \frac{1}{\sin(\theta)}. \tag{1.19}$$

So $\eta^F_{\min}(K)$ is large if the triangle $(F(a), F(b), F(c))$ is flat (all its interior angles are close to 0 or π). We define

$$\eta^*_{\min} := \sup_{K\in\mathcal{T}_h} \eta^F_{\min}(K). \tag{1.20}$$

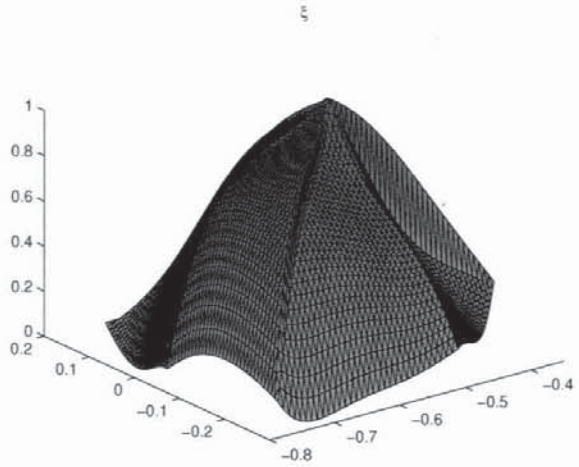

FIGURE 1.5. Localized Galerkin elements ξ_i.

Let us recall that although the coefficients of the PDE (1.1) are irregular, it is well-known [70] that F is Hölder-continuous. Thus it makes sense to look at the value of F at a specific point. Now let v be a function defined on the nodes of the triangle $K \in \mathcal{T}_h$, and let us denote by a, b, and c the nodes of that triangle. It is usual to look at the coarse gradient of v evaluated at the nodes of the triangle K, i.e., the vector defined by

$$\nabla v(K) := \begin{pmatrix} b-a \\ c-a \end{pmatrix}^{-1} \begin{pmatrix} v(b)-v(a) \\ v(c)-v(a) \end{pmatrix}. \tag{1.21}$$

If $\eta^F_{\min}(K) < \infty$, then the following object, called the gradient of v evaluated on the coarse mesh with respect to the metric induced by F, is well-defined:

$$\nabla_F v(K) := \begin{pmatrix} F(b)-F(a) \\ F(c)-F(a) \end{pmatrix}^{-1} \begin{pmatrix} v(b)-v(a) \\ v(c)-v(a) \end{pmatrix}. \tag{1.22}$$

DEFINITION 1.25 We say that the tessellation $\mathcal{T}_h$ is *not unadapted* to F if and only if the determinant of $\nabla F(K)$ is strictly positive for all $K \in \mathcal{T}_h$.

Remark 1.26. Note that if the tessellation $\mathcal{T}_h$ is not unadapted to F then $\eta^*_{\min}(K) < \infty$; Definition 1.25 contains the additional condition that there is no inversion in the images of the triangles of $\mathcal{T}_h$ by F.

Now consider the nodal elements $(\xi_i)_{i \in \mathcal{N}_h}$ defined by

$$\begin{cases} \xi_i(x_j) = \delta_{ij} \\ \nabla_F \xi(x) = \text{constant within each } K \in \mathcal{T}_h. \end{cases} \tag{1.23}$$

If the mesh is not unadapted to F, then the elements (Figure 1.5) (1.23) are well-

defined and given by

$$\begin{cases} \xi_i(x) = 1 + (F(x) - F(x_i))\nabla_F \varphi_i(K) & \text{if } i \sim K \text{ and } x \in K \\ \xi_i(0) = 0 & \text{in other cases} \end{cases} \tag{1.24}$$

where the notation $i \sim K$ means that i is a node of K. Observe that the elements ξ_i are discontinuous at the boundaries of the triangles of the coarse mesh; however, they are easier to implement since they are localized in these triangles. Denote by Z_h the vector space spanned by the functions ξ_i. For $K \in \mathcal{T}_h$ we denote by a_K the bilinear form on $H^1(K)$ defined by

$$a_K[v, w] := \int_K {}^{\mathsf{T}}\nabla v a \nabla w. \tag{1.25}$$

We will denote by $H^1(\mathcal{T}_h)$ the space of functions $v \in L^2(\Omega)$ such that the restriction of v to each triangle K belongs to $H^1(K)$. We will write for $v, w \in H^1(\mathcal{T}_h)$

$$a^*[v, w] := \sum_{K \in \mathcal{T}_h} a_K[v, w]. \tag{1.26}$$

The localized finite element method can be formulated in the following way: look for $u^f \in Z_h$ such that for all $i \in \mathcal{N}_h$,

$$a^*[\xi_i, u^f] = (\xi_i, g)_{L^2(\Omega)}. \tag{1.27}$$

We have the following estimate:

THEOREM 1.27 *Assume that σ is stable and that the mesh is not unadapted to F. Then there exists a constant $\alpha > 0$ such that*

$$(a^*[u - u^f])^{1/2} \leq C\eta^*_{\min} h^\alpha \|g\|_{L^\infty(\Omega)}. \tag{1.28}$$

Remark 1.28. For a bilinear from $B[\,\cdot\,,\cdot\,]$ we write $B[v] := B[v, v]$.

Remark 1.29. The constant α depends only on n, Ω, ϵ, and μ_σ. The constant C depends on the objects mentioned above plus $\|(\mathrm{tr}(\sigma))^{-1-\epsilon}\|_{L^1(\Omega)}$.

Remark 1.30. The bilinear operator $a^*[\,\cdot\,,\cdot\,]$ on Z_h is characterized by a constant matrix within each triangle $K \in \mathcal{T}_h$ equal to

$${}^{\mathsf{T}}(\nabla F(K))^{-1} \langle {}^{\mathsf{T}}\nabla F a \nabla F \rangle_K (\nabla F(K)) \tag{1.29}$$

where $\langle v \rangle_K$ means the average of v over K with respect to the Lebesgue measure ($\langle v \rangle_K := \frac{1}{\mathrm{vol}(K)} \int_K v(x)dx$, $\mathrm{vol}(K)$ being the Lebesgue measure of volume of K).

The error bound given in Theorem 1.27 is given in the norm induced by $a^*[\,\cdot\,,\cdot\,]$. We would like to obtain an error bound with respect to the usual H^1-norm. Observe that u^f is discontinuous at the boundaries of the triangles of the coarse mesh, so we have to find an accurate way to interpolate u^f in the whole space using its values at the nodes of the coarse mesh. Let us denote by $F(\mathcal{N}_h)$ the image of the nodes of $\mathcal{T}_h$ by F.

Let $\mathcal{T}^F$ represent the triangulation of $F(\mathcal{N}_h)$. Let φ_i^F be the standard piecewise linear nodal basis of $\mathcal{T}^F$. Let us denote by $\mathcal{J}_h$ the interpolation operator from the space of functions defined on the nodes of $\mathcal{T}_h$ into $H^1(\Omega)$ defined by

$$\mathcal{J}_h v(x) := \sum_{i \in \mathcal{N}_h} v(x_i) \varphi_i^F \circ F(x). \tag{1.30}$$

Observe that for $i \in \mathcal{N}_h$, $v(x_i) = \mathcal{J}_h v(x_i)$. We have the following estimate:

THEOREM 1.31 *Assume that σ is stable and that the mesh is not unadapted to F. Then there exist constants $\alpha, C_f > 0$ such that*

$$\|u - \mathcal{J}_h u^f\|_{H^1(\Omega)} \leq C_f h^\alpha \|g\|_{L^\infty(\Omega)}. \tag{1.31}$$

Remark 1.32. The constant α depends only on n, Ω, and μ_σ. The constant C_f can be written

$$C_f := C\eta_{\min}^* \big(\min(\eta_{\max}^* \eta_{\max}^3, \nu^*) \big)^{1/2} \tag{1.32}$$

where C depends on the objects mentioned above plus $\|(\mathrm{tr}(\sigma))^{-1-\epsilon}\|_{L^1(\Omega)}$, $\lambda_{\min}(a)$, and $\lambda_{\max}(a)$. The quantity $\eta_{\max}$ is defined by $1/\sin\theta$ where θ is the interior angle of the triangles of $\mathcal{T}_h$ closest to 0 or π, and $\eta_{\max}^*$ is defined by $1/\sin\gamma$ where γ is the interior angle of the triangles of $\mathcal{T}^F$ closest to 0 or π. Moreover,

$$\nu^* := \sup_{K \in \mathcal{T}_h} \frac{\mathrm{vol}(K^F)}{\mathrm{vol}(F(K))} \tag{1.33}$$

where K^F is the triangle whose nodes are the images of the nodes of K by F.

1.4 Numerical Homogenization from the Information Point of View

The Galerkin scheme described in Sections 1.2 and 1.3 are based on elements containing the whole fine-scale structure of F. This represents too much information. We can wonder what minimal quantity of information should be kept from the scales in order to upscale (1.1). We would like to keep an accurate version of (1.1) with minimal computer memory. This point touches the compression issue. Images can be compressed. Can the same thing be done with operators?

This question has received an answer within the context of the fast multiplication of vectors with fully populated special matrices arising in various applications [36]. Let us recall the fast multipole method and the hierarchical multipole method designed by L. Greengard and V. Rokhlin [44]. Wavelet-based methods have been designed by G. Beylkin, R. Coifman, and V. Rokhlin [3, 17, 16]. The concept of hierarchical matrices has been developed by W. Hackbusch et al. [46]. More precisely, we refer to [9, 10, 11, 12, 13].

The hierarchical matrix method is based on a compression of the inverse of the stiffness matrix (see Remark 1.22). Here we consider compression from the point of view of numerical homogenization. We look at the operator (1.1) as a

bilinear form on $H_0^1(\Omega)$, and we will use V_h as space of test functions to *zoom at* the operator associated to a at a given arbitrary resolution:

$$a : \begin{cases} H_0^1(\Omega) \times H_0^1(\Omega) \to \mathbb{R} \\ (v, w) \to \int_\Omega {}^{\mathsf{T}}\nabla v a \nabla w. \end{cases} \tag{1.34}$$

The upscaled or compressed operator, written $\mathcal{U}_h a$, will naturally be a bilinear form on the space of piecewise linear functions on the coarse mesh with Dirichlet boundary condition:

$$\mathcal{U}_h a : \begin{cases} V_h \times V_h \to \mathbb{R} \\ (v, w) \to \mathcal{U}_h a[v, w]. \end{cases} \tag{1.35}$$

The question is how to choose $\mathcal{U}_h a$. To answer that question we can integrate (1.1) against a test function ϕ in V_h; then we obtain that

$$\int_\Omega \nabla \phi a \nabla u = \int_\Omega \phi g. \tag{1.36}$$

We will use the test function ϕ to "look at" the operator (1.1) at the given resolution h. We can decompose the first term in the integral above as a sum of integrals over the triangles of the coarse mesh to obtain (we assume that σ is stable)

$$\int_\Omega \nabla \phi a \nabla u = \sum_{K \in \mathcal{T}_h} \int_K \nabla \phi(x) a(x) \nabla F(x) (\nabla F(x))^{-1} \nabla u(x) dx. \tag{1.37}$$

Now $\nabla \phi$ is constant within each triangle $K \in \mathcal{T}_h$. $(\nabla F(x))^{-1} \nabla u(x)$ is Hölder-continuous and thus almost a constant within each triangle K and equal to the gradient of u evaluated on the coarse mesh with respect to the metric induced by F, i.e., the following vector:

$$\nabla_F u(K) := \begin{pmatrix} F(b) - F(a) \\ F(c) - F(a) \end{pmatrix}^{-1} \begin{pmatrix} u(b) - u(a) \\ u(c) - u(a) \end{pmatrix} \tag{1.38}$$

where a, b, and c are the nodes of the triangle K. It follows that the tensor $a \nabla F$ can be averaged over each triangle of the coarse mesh, and we will denote by $\langle a \nabla F \rangle_K$ its average. In conclusion, a good candidate for the upscaled operator $\mathcal{U}_h a$ is the bilinear form given by the following formula: for $v, w \in V_h$

$$\mathcal{U}_h a[v, w] := \sum_{K \in \mathcal{T}_h} \int_K {}^{\mathsf{T}}\nabla v \langle a \nabla F \rangle_K (\nabla F(K))^{-1} \nabla w. \tag{1.39}$$

Observe that the only information kept from the small scales in the compressed operator (1.39) are the bulk quantities $\langle a \nabla F \rangle_K$ and the nonaveraged quantities $F(b) - F(a)$ where a and b are nodes of the triangles of the coarse mesh. The latter quantity can be interpreted as a deformation of the coarse mesh induced by the small scales (or a new distance defining coarse gradients). In the particular case where $a = M(x/\epsilon)$ and M is ergodic, then as $\epsilon \downarrow 0$ $\langle a \nabla F \rangle_K$ converges to

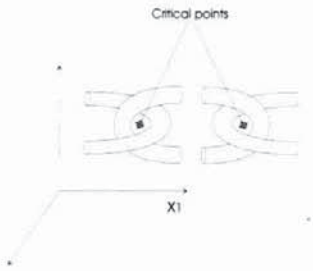

FIGURE 1.6. a in dimension 3.

the usual effective conductivity obtained from homogenization theory and $\nabla F(K)$ converges to the identity matrix. It follows that the object (1.39) recovers the formulae obtained from homogenization theory when the medium is ergodic and characterized by scale separation. Let us now show that formula (1.39) can be accurate beyond these assumptions.

To estimate the compression accuracy, we have to use the upscaled operator $\mathcal{U}_h a$ to obtain an approximation of the linear interpolation of u on the coarse mesh. We look for $u^m \in V_h$ such that for all $i \in \mathcal{N}_h$,

$$\mathcal{U}_h a[\varphi_i, u^m] = (\varphi_i, g)_{L^2(\Omega)}. \tag{1.40}$$

The price to pay for the loss of information on the small scales is the loss of ellipticity. This loss can be caused by two correlated factors:

- the new metric can generate flat triangles and
- the upscaled operator can become singular.

The first factor is due to the localization of the scheme. The second factor does not appear with Galerkin schemes. It is not observed in dimension 2, but it can't be avoided in higher dimensions in the sense that the upscaled operator has no reason to remain elliptic and local.

Indeed, consider a box of dimension 3, and set in that box empty tubes of low boundary conductivity, as shown in Figure 1.6. Set the left side of the box to temperature 0°C and the right side to temperature 100°C. Then an inversion in the temperature profile is produced around the critical points shown in Figure 1.6 (see [4, 21]; instead of increasing from left to right in these regions the temperature decreases). Now as the operator is upscaled, the information on the geometry of the tubes is lost but the inversion phenomenon remains in the loss of ellipticity and locality of the operator. We will address this issue further in a forthcoming paper.

Nevertheless, it is possible to prove that once stability is achieved, then the method is accurate (if σ is stable). More precisely, for a nodal function v, let us define the homogeneous Dirichlet form on the graph induced by $\mathcal{T}_h$:

$$\mathcal{E}_h[v] := \sum_{i \sim j} |v_i - v_j|^2. \tag{1.41}$$

We write $i \sim j$ when those nodes share an edge on the coarse mesh. Let us define the following stability parameter of the scheme:

$$\mathcal{S}^m := \inf_{w \in V_h} \sup_{v \in V_h} \frac{\mathcal{U}_h a[v, w]}{(\mathcal{E}_h[v])^{1/2} (\mathcal{E}_h[w])^{1/2}}. \tag{1.42}$$

Observe that $\mathcal{S}^m$ depends only on the upscaled parameters so we have a control on the stability.

DEFINITION 1.33 We say that the scheme is *stable* if and only if $\mathcal{S}^m > 0$.

Remark 1.34. Let us recall that for $v \in V_h$, $\mathcal{E}_h[v]$ can be bounded from below and above by the L^2-norm of the gradient of v. More precisely,

$$\frac{1}{4\eta_{\max}} \mathcal{E}_h[v] \leq \|\nabla v\|^2_{L^2(\Omega)} \leq \eta_{\max} \mathcal{E}_h[v], \tag{1.43}$$

where $\eta_{\max} = 1/\sin\theta$ and θ is the closest interior angle of the triangles of $\mathcal{T}_h$ to 0 or π.

Remark 1.35. In practice, in dimension 2 the condition number of the scheme associated to the upscaled operator is as good as the one obtained from a Galerkin scheme by solving a local cell problem.

Let us denote by $\mathcal{I}_h u$ the linear interpolation of u over $\mathcal{T}_h$:

$$\mathcal{I}_h u := \sum_{i \in \mathcal{N}_h} u(x_i) \varphi_i(x). \tag{1.44}$$

We have the following estimate:

THEOREM 1.36 *Assume that σ and the scheme are stable and that the mesh is not unadapted to F. Then there exist constants $\alpha, C_m > 0$ such that*

$$\|\mathcal{I}_h u - u^m\|_{H^1(\Omega)} \leq C_m h^\alpha \|g\|_{L^\infty(\Omega)}. \tag{1.45}$$

Remark 1.37. The constant α depends only on n, Ω, and μ_σ. The constant C_m can be written as

$$C_m := C \frac{\eta^*_{\min} \eta_{\max}}{\mathcal{S}^m}, \tag{1.46}$$

where C depends on the objects mentioned above plus $\|(\mathrm{tr}(\sigma))^{-1-\epsilon}\|_{L^1(\Omega)}$, $\lambda_{\min}(a)$, and $\lambda_{\max}(a)$.

The compressed operator allows us to capture the solution of (1.1) on a coarse mesh (Figure 1.7). What information should be added to the compressed operator in order to obtain fine-resolution approximation of u? The answer is a finer resolution of F (Figure 1.8). Indeed, let $\mathcal{J}_h$ be the interpolation operator introduced in (1.30); we then have the following estimate:

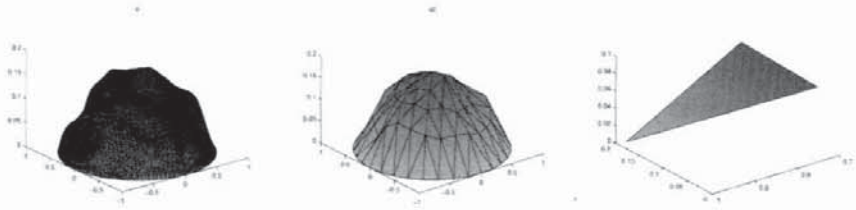

(a) u. (b) u^m. (c) Triangle of the coarse mesh.

FIGURE 1.7. u estimated with the upscaled operator.

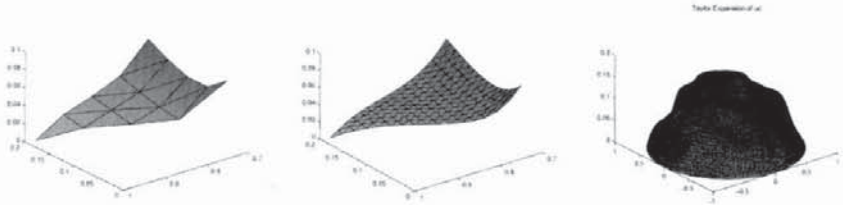

(a) Refined F. (b) Refined F. (c) $\mathcal{J}_h u$.

FIGURE 1.8. Taylor expansion with respect to the new metric.

THEOREM 1.38 *Assume that σ and the scheme are stable and that the mesh is not unadapted to F. Then there exist constants $\alpha, C_m > 0$ such that*

$$\|u - \mathcal{J}_h u^m\|_{H^1(\Omega)} \leq C_m h^\alpha \|g\|_{L^\infty(\Omega)}. \tag{1.47}$$

Remark 1.39. The constant α depends only on n, Ω, and μ_σ. The constant C_m can be written

$$C_m := C\left(\frac{\eta^*_{\max}\eta_{\max}}{S^m}\right)^{1/2} \tag{1.48}$$

where C depends on the objects mentioned above plus $\|(\mathrm{tr}(\sigma))^{-1-\epsilon}\|_{L^1(\Omega)}$, $\lambda_{\min}(a)$, and $\lambda_{\max}(a)$.

We want to compress a physical system from a fine-scale description (F) to a coarse-scale description (C). There are two ways of doing so:

- either we upscale directly from (F) to (C) or
- we do so in two steps: from (F) to an intermediate scale (I) and then from (I) to (C).

Now if the scales (F), (I), and (C) are not completely separated, a technique based solely on averaging (upscaling of bulk quantities) will produce two different results (depending on the presence of an intermediate step). Thus it is important to check the consistency of the numerical homogenization method if the metric information $F(x_i) - F(x_j)$ is upscaled in addition to traditional bulk quantities $\langle a \nabla F \rangle_K$.

Let $\mathcal{T}^0, \ldots, \mathcal{T}^n$ be a multiresolution tessellation of Ω. Each $\mathcal{T}^i$ is a regular conformal tessellation of Ω. Moreover, $\mathcal{T}^{i+1}$ is a refinement of $\mathcal{T}^i$. Let us denote by V^i the space of piecewise linear functions on $\mathcal{T}^i$. We denote by $\mathcal{B}^i$ the space of bilinear operators on $\mathcal{T}^i$. We want to compress (upscale) the bilinear operator $a[\cdot, \cdot]$ on the multigrid $\mathcal{T}^0, \ldots, \mathcal{T}^n$. We assume that the smallest scale n is fine enough to capture the irregularities of a; in that case we define a^n such that for all $v, u \in V^n$

$$a^n[v, u] := a[v, u]. \tag{1.49}$$

Since the gradient of an element of V^n is constant within each triangle of $\mathcal{T}^n$, $a^n[\cdot, \cdot]$ can be defined by a mapping from $\mathcal{T}^n$ onto $\mathcal{M}_n$, the space of $n \times n$ constant matrices. We will denote by $a^n(K)$ the constant matrix associated to $K \in \mathcal{T}^n$.[3] Similarly, each bilinear operator of $\mathcal{B}^i$ can be defined by mapping from $\mathcal{T}^i$ onto $\mathcal{M}_n$. We define, for $k \leq p$, $\mathcal{U}^{k,p}$, the upscaling operator mapping $\mathcal{B}^p$ onto $\mathcal{B}^k$ in the following way (we assume that the tessellations $\mathcal{T}_i$ are not unadapted to F and that the respective schemes are stable). Let $B \in \mathcal{B}^p$.

- Let $F \in V^p$ be the solution of

$$\begin{cases} B[v, F] = 0 & \text{for all } v \in V^p \\ F = x & \text{on } \Gamma^i \end{cases} \tag{1.50}$$

  where we have denoted by Γ^i the boundary of $\mathcal{T}^i$.
- The bilinear form $\mathcal{U}^{k,p}B$ is defined by its matrices $\mathcal{U}^{k,p}B(K)$ for $K \in \mathcal{T}^k$:

$$\mathcal{U}^{k,p}B(K) := \langle B\nabla F\rangle_K (\nabla F(K))^{-1}. \tag{1.51}$$

  $\langle \cdot \rangle$ stands for the averaging operator

$$\langle B\nabla F\rangle_K := \frac{1}{\operatorname{vol}(K)} \sum_{T \in \mathcal{T}^p, T \subset K} \operatorname{vol}(T) B(T) \nabla F(T). \tag{1.52}$$

For $k \leq p \leq q$, $\mathcal{U}$ satisfies the semigroup property

$$\mathcal{U}^{k,q} = \mathcal{U}^{k,p}\mathcal{U}^{p,q}. \tag{1.53}$$

Note also that $\mathcal{U}^{q,q} = I_d$. In particular, if we define for $k \in \{1, \ldots, n\}$

$$a^k := \mathcal{U}^{k,n} a^n \tag{1.54}$$

as the upscaled operator, the following semigroup property is satisfied: for $k \leq p \leq n$

$$a^k := \mathcal{U}^{k,p} a^p. \tag{1.55}$$

Semigroup properties (1.53) and (1.55) are essential to the consistency and coherence of the numerical homogenization method.

[3] The bilinear form (1.49) can be written as a sum of integrals over $K \in \mathcal{T}^n$. The quantities ∇v and ∇u are constant over these triangles; thus a^n_K as a bilinear form over V^n is determined by a matrix.

1.5 Numerical Homogenization from the Transport Point of View

The elliptic operator appearing in (1.1) can be seen as the generator of a stochastic differential equation. This stochastic differential equation can reflect the transport process of a pollutant in a highly heterogeneous medium such as soil. The operator $\Delta - \nabla V \nabla$, whose numerical homogenization is similar to that of (1.1), can represent a physical system evolving in a highly irregular energy landscape V. The simple fact that this evolution taking place in a continuous domain can be captured by a Markov chain evolving on a graph is far from being obvious [72]. Our point of view here is to accurately simulate a Markov chain living on a fine graph by an "upscaled" Markov chain living on a coarse graph. The main question is how to choose the jump rate γ_{ij} of the random walk between the nodes of the coarse graph. The answer is given by a finite-volume method.

Let us denote by $\mathcal{T}_h^*$ the dual mesh associated to $\mathcal{T}_h$. $\mathcal{T}_h^*$ can be obtained by drawing segments from the midpoints of the edges of the triangles of $\mathcal{T}_h$ to an interior point in these triangles (the circumcenter to obtain a Voronoï tessellation, but one can also choose the barycenter).

Let us denote by V_i the control volume associated to the node i of the primal mesh and χ_i the characteristic function of V_i. The finite-volume method can be expressed in the following way: look for $u^v \in \mathcal{Z}_h$ ($\mathcal{Z}_h$ being the space spanned by the elements ξ_i introduced in (1.23)) such that for all $i \in \mathcal{N}_h$

$$a^*[\chi_i, u^v] = (\chi_i, g)_{L^2}. \tag{1.56}$$

Again, it follows from equation (1.56) that the only information kept from the scales are the usual bulk quantities (effective conductivities at the edges of the dual mesh) plus the metric information $F(b) - F(a)$, where a and b are nodes of the triangles of the primal mesh. Observe also that it is possible to generate with this finite-volume method a coherent multiresolution compression similar to the one introduced in Section 1.4. According to (1.56) the good choice for the jump rates of the random walk should be

$$\gamma_{ij} = a^*[\chi_i, \xi_j] \quad \text{if } i \sim j \text{ and } i \neq j. \tag{1.57}$$

To properly describe the transport process, one should look at a parabolic operator instead of the elliptic one. This issue will be addressed in [67]; we will restrict ourselves to the elliptic case characterizing the equilibrium properties of the random walk. Let us denote by $\mathcal{S}^v$ the stability of the upscaled finite-volume operator. It is defined by

$$\mathcal{S}^v := \inf_{w \in \mathcal{Z}_h} \sup_{v \in \mathcal{Y}_h} \frac{a^*[v, w]}{(\mathcal{E}_h[v])^{1/2} (\mathcal{E}_h[w])^{1/2}}. \tag{1.58}$$

THEOREM 1.40 *Assume that σ and the scheme are stable ($S^v > 0$) and that the mesh is not unadapted to F. Then there exist constants $\alpha, C_v > 0$ such that*

$$\|\mathcal{I}_h u - \mathcal{I}_h u^v\|_{H^1(\Omega)} \leq C_{v,1} h^\alpha \|g\|_{L^\infty(\Omega)} \tag{1.59}$$

and

$$\|u - \mathcal{J}_h u^v\|_{H^1(\Omega)} \leq C_{v,2} h^\alpha \|g\|_{L^\infty(\Omega)}. \tag{1.60}$$

Remark 1.41. The constant α depends only on n, Ω, and μ_σ. The constant $C_{v,1}$ can be written

$$C_{v,1} := C \frac{\eta^*_{\min} \eta_{\max}}{S^m} (\lambda_{\max}(\sigma))^{1/2}. \tag{1.61}$$

The constant $C_{v,2}$ can be written

$$C_{v,2} := C \left(\frac{\lambda_{\max}(\sigma) \eta^*_{\max} \eta_{\max}}{S^v} \right)^{1/2}. \tag{1.62}$$

The constant C depends on the objects mentioned above plus $\|(\mathrm{tr}(\sigma))^{-1-\epsilon}\|_{L^1(\Omega)}$, $\lambda_{\min}(a)$, and $\lambda_{\max}(a)$.

Remark 1.42. Observe that we need the additional condition $\lambda_{\max}(\sigma) < \infty$ to prove the convergence of the method. Numerical experiments show that although the finite-volume method keeps very little information from small scales, it is more stable and accurate than the method presented in Section 1.4 (it is also more stable and almost as accurate as the Galerkin method, in which the whole fine-scale structure of F is upscaled). That is why we believe that the constants in (1.61) and (1.62) are not optimal.

1.6 Explicit Formulae in Laminar Cases

The harmonic coordinates can be explicitly computed in dimension 1. In this section we will analyze a toy model to understand the effect of the new metric when the coefficients of the partial differential equations are characterized by an infinite number of overlapping scales. Our point is to show that the new metric becomes multifractal.

Let $\Omega := (0, 1)$. Let $V \in L^\infty(\Omega)$, and let $w(V)$ denote the weak solution of the following Dirichlet problem:

$$\begin{cases} -\frac{1}{2} e^{2V} \operatorname{div}(e^{-2V} \nabla w) = f \\ w = 0 \qquad\qquad\qquad\qquad \text{on } \partial\Omega. \end{cases} \tag{1.63}$$

With $f \in L^\infty(\Omega)$. We denote by $w(V)$ the solution of (1.63). Denote by μ_+ and μ_- the probability measures defined on the Borelian subset of $(0, 1)$:

$$\mu_+[0, x] := \frac{\int_0^x e^{2V(z)}\, dz}{\int_0^1 e^{2V(z)}\, dz} \quad \text{and} \quad \mu_-[0, x] := \frac{\int_0^x e^{-2V(z)}\, dz}{\int_0^1 e^{-2V(z)}\, dz}. \tag{1.64}$$

Define $D(V) := (\int_0^1 e^{2V(z)} dz \int_0^1 e^{-2V(z)} dz)^{-1}$. Observe that in dimension 1, $a \nabla F$ is a constant and is equal to $D(V)$. Observe that (1.63) can be explicitly rewritten

$$-\frac{1}{2} \frac{d}{d\mu_-} D(V) \frac{d}{d\mu_+} u = f. \tag{1.65}$$

In that sense the metric-based numerical homogenization is exact in dimension 1. Equations such as (1.65) have been studied in dimension 1 in [39, 40] in order to introduce a measure-theoretic way of defining differential operators on fractal sets on the real line.

Let V_n be a sequence in $L^\infty(\Omega)$. We call a probability measure *nondegenerate* if and only if it is atomless and the mass of any nonvoid open subset of Ω is strictly positive. We have the following theorem:

THEOREM 1.43 *If $\mu_+^{V_n}$ and $\mu_-^{V_n}$ weakly converge to nondegenerate probability measures μ_+ and μ_-, then $D(V_n)w(V_n)$ converges pointwise to the unique solution of the following differential equation with Dirichlet boundary condition*:

$$-\frac{1}{2}\frac{d}{d\mu_-}\frac{d}{d\mu_+}\psi = f. \tag{1.66}$$

In the case of classical homogenization, note that μ_+ and μ_- are simple Lebesgue probability measures on $[0, 1]$.

Let $\mathbb{T}$ denote the torus of dimension 1 and side of length 1, and let $U \in C^1(\mathbb{T})$. Let $\rho \in \mathbb{N}/\{0, 1\}$. Denote by T_ρ the scaling operator denied on the space of functions by $T_\rho U(x) := U(\rho x)$, and let

$$S_n U := \sum_{p=0}^{n-1} T_{\rho^p} U. \tag{1.67}$$

Take $V_n = S_n U$ in Theorem 1.43. Then by the Perron-Frobenius-Ruelle theorem [78], $\mu_+^{V_n}$ and $\mu_-^{V_n}$ weakly converge to some probability measure μ_+ and μ_- (eigenvectors of the Ruelle transfer operator), and it is easy to check that they are nondegenerate. Let us note that similarly it is possible to show that $-\frac{1}{n}\ln D(V_n)$ converges to the sum of topological pressures of U and $-U$ with respect to the shift induced by the multiplication by ρ on the space of ρ-adic decompositions [14, 65].

Theorem 1.43 says that the regularity of ψ corresponds to the regularity of $\mu_+[0, x]$; thus it is natural to wonder what the regularity of that harmonic measure is. To answer that question, we will consider the paradigm of binomial measures. We refer to [68] for a detailed introduction to this subject; for the sake of completeness we will recall its main lines below in our framework. We take $U(x) \in L^\infty(\mathbb{T})$ with $(a \neq b)$

$$2U(x) = \begin{cases} a & \text{for } 0 \leq x < \frac{1}{2} \\ b & \text{for } \frac{1}{2} \leq x < 1. \end{cases} \tag{1.68}$$

Let us write

$$m_0 = \frac{e^a}{e^a + e^b} \quad \text{and} \quad m_1 = \frac{e^b}{e^a + e^b}. \tag{1.69}$$

Then $\mu_+^{V_n}$ weakly converges to μ_+, and that measure is self-similar in the sense that it satisfies

$$\mu_+([x, y]) = m_0\mu_+([2x, 2y]) + m_1\mu_+([2x - 1, 2y - 1]). \tag{1.70}$$

For $x \in (0, 1)$ we denote by $x_1x_2\cdots$ its 2-adic decomposition in the sense that $x = \sum_{n=0}^{\infty} x_n 2^n$. We denote by $I_{y_1,\ldots,y_p}$ the cylinder of $x \in (0, 1)$ such that $x_1 \cdots x_p = y_1 \cdots y_p$. μ_+ is atomless but singular with respect to Lebesgue measure. Moreover, it is easy to check [68] that μ_+ and therefore ψ are Holder-continuous and their Holder continuity exponent is not a constant.

More precisely, let us write

$$\alpha_n(x) := -\frac{\ln(\mu_+[I_{x_1,\ldots,x_n}])}{n \ln 2} \tag{1.71}$$

and

$$\alpha(x) := \lim_{n\to\infty} \alpha_n(x) \tag{1.72}$$

whenever this limit exists. This limit exists for almost all x (with respect to Lebesgue measure), and its value depends on the dyadic expansion of x. Denoting by $l_n(x)$ the number of ones appearing in the first n digits of x, we have

$$\alpha(x) = \lim_{n\to\infty} -\left(1 - \frac{l_n(x)}{\ln n}\right)\log_2(m_0) - \frac{l_n(x)}{\ln n}\log_2(m_1). \tag{1.73}$$

Thus $\alpha(x)$ can take all the values between $-\log_2(m_0)$ and $-\log_2(m_1)$. However, for almost all x with respect to Lebesgue measure,

$$\alpha(x) = -\frac{1}{2}\log_2(m_0m_1) = -\frac{1}{\ln 2}\left(\frac{a+b}{2} - \ln(e^a + e^b)\right). \tag{1.74}$$

Now it is possible to obtain from large-deviation theory ([32] and theorem 2, of [68]) that

$$\mathbb{P}(\alpha_n(x) \in (\alpha - \epsilon, \alpha + \epsilon)) \to 1 + c^*(\alpha), \tag{1.75}$$

$\mathbb{P}$ being the uniform probability measure on $(0, 1)$, $c(q) = 1 - \log_2(m_0^q + m_1^q)$, and c^* denoting the Legendre transform of c, i.e., $c^*(\alpha) = \inf_q(q\alpha - c(q))$. Thus the metric associated to our upscaling method is multifractal [25, 41, 52]. Let us recall that multifractal formalism was originally introduced to describe the regularity of the velocity field in turbulence [41] and to explain intermittency.

1.7 Literature

The issue of numerical homogenization partial differential equations with heterogeneous coefficients has received a great deal of attention and many methods have been proposed.[4] Let us mention a few of them:

[4] Wavelet-based methods have been justified in dimension 1. Multiscale finite element methods have been justified in periodic media under scale separation. Heterogeneous multiscale methods have been justified in locally ergodic media under the assumption of scale sparation.

- multiscale finite element methods [2, 31, 37, 43, 47, 50, 64]
- multiscale finite volume methods [53]
- heterogeneous multiscale methods [30]
- wavelet-based homogenization [7, 18, 19, 23, 29, 42]
- residual free bubbles methods [20]
- discontinuous enrichment methods [34, 35]
- partition-of-unity methods [38]
- energy-minimizing multigrid methods [75].

The methods mentioned above are part of a larger quest aimed at capturing high-dimensional problems with a few coarse parameters [5, 45, 62, 69] . Paraphrasing the outcome of a recent DOE workshop [28], we may understand the physics of multiscale structures at each individual scale; nevertheless, *without the ability to "bridge the scales," a significant number of important scientific and engineering problems will remain out of reach.*

2 Proofs

2.1 Compensation

Let us prove Theorem 1.4. We need a variation of Campanato's result [22] on non-divergence-form elliptic operators. Let us write for a symmetric matrix M,

$$\nu_M := \frac{\sum_{i=1}^n \lambda_{i,M}}{\sum_{i=1}^n \lambda_{i,M}^2}. \tag{2.1}$$

We consider the following Dirichlet problem:

$$L_M v = f \tag{2.2}$$

with $L_M := \sum_{i,j=1}^n M_{ij}(x)\partial_i\partial_j$. We assume M to be elliptic and symmetric.

THEOREM 2.1 *Assume that $\beta_M < 1$. If Ω is convex, then there exists a real number $p > 2$ depending only on n, Ω, and β_M such that if $f \in L^p(\Omega)$ the Dirichlet problem* (2.2) *has a unique solution satisfying*

$$\|v\|_{W_0^{2,p}(\Omega)} \leq \frac{C}{1-\beta_M^{1/2}} \|\nu_M f\|_{L^p(\Omega)}. \tag{2.3}$$

Remark 2.2. β_M is the Cordes parameter (1.8) associated to M.

PROOF: Theorem 2.1 is a straightforward adaptation of theorem 1.2.1 of [57]; for the sake of completeness we will give the main lines of ideas leading to estimate (2.3). Let us recall the Miranda-Talenti estimate [57].

LEMMA 2.3 *Let $\Omega \subset \mathbb{R}^n$ be a bounded and convex domain of class C^2. Then for each $v \in W_0^{2,2}(\Omega)$ we get the result*

$$\int_\Omega \sum_{i,j=1}^n (\partial_i\partial_j v)^2\, dx \leq \int_\Omega (\Delta v)^2\, dx. \tag{2.4}$$

The Laplacian $\Delta : W_0^{2,p}(\Omega) \to L^p(\Omega)$ is an isomorphism for each $p > 1$. Let $\Delta^{-1}(p)$ be the inverse operator $\Delta^{-1} : L^p(\Omega) \to W_0^{2,p}$. It is clear from (2.4) that $\|\Delta^{-1}(2)\| \leq 1$. Let $r \in (2, \infty)$; by the convexity of the norms we have

$$\|\Delta^{-1}(p)\| \leq C(p) \tag{2.5}$$

with

$$C(p) := \|\Delta^{-1}(r)\|^{\frac{r(p-2)}{p(r-2)}}. \tag{2.6}$$

Letting v be a solution of (2.2) (we refer to [57] for the existence of v, which is obtained from a fixed-point theorem), we have

$$\|v\|_{W_0^{2,p}(\Omega)} \leq \|\Delta^{-1}(p)\| \, \|\Delta v\|_{L^p(\Omega)}. \tag{2.7}$$

Observing that $\Delta v = \nu_M f + \Delta v - \nu_M L_M v$, we can obtain

$$\|\Delta v\|_{L^p(\Omega)} \leq \|\nu_M f\|_{L^p(\Omega)} + \|\Delta v - \nu_M L_M v\|_{L^p(\Omega)}. \tag{2.8}$$

Then, following the proof of theorem 1.2.1 of [57], we have

$$\|\Delta v - \nu_M L_M v\|_{L^p(\Omega)}^p \leq \int_\Omega \beta_M^{p/2} \Big(\sum_{i,j=1}^n (\partial_i \partial_j v)^p \Big) dx. \tag{2.9}$$

Let us choose $p > 2$ such that $1 - C(p)\beta_M^{1/2} \geq (1 - \beta_M^{1/2})/2$. Combining (2.7), (2.8), and (2.9) we obtain that

$$\Big(\int_\Omega \Big(\sum_{i,j=1}^n (\partial_i \partial_j v)^p \Big) dx \Big)^{1/p} \leq \frac{2C(p)}{1 - \beta_M^{1/2}} \|\nu_M f\|_{L^p(\Omega)}, \tag{2.10}$$

which leads to estimate (2.3). □

Remembering the Sobolev embedding inequality

$$\|\nabla v\|_{C^{1-n/p}(\bar{\Omega})} \leq C \|v\|_{W_0^{2,p}(\Omega)}, \tag{2.11}$$

Theorem 2.1 implies the Hölder continuity of v in dimension $n = 2$.

We assume that σ is stable. We denote by F^{-1} the inverse of F (which is well-defined if σ is stable). Let Q denote the symmetric positive matrix given by the equation

$$Q(y) := \left(\frac{({}^{\mathrm{T}}\nabla F a \nabla F)}{|\det(\nabla F)|} \right) \circ F^{-1}(y), \tag{2.12}$$

and let w denote the solution of the following equation: for all $\hat{\varphi} \in C_0^\infty$,

$$\sum_{i,j=1}^n Q_{ij} \partial_i \partial_j w = -\frac{\hat{g}}{|\det(\nabla F)| \circ F^{-1}}. \tag{2.13}$$

Let us now prove the following theorem:

THEOREM 2.4 *Assume that σ is stable and that Ω is convex. Then there exists constants $p > 2$ and $C > 0$ such that the solution of* (2.13) *belongs to* $W_0^{2,p}(\Omega)$ *and satisfies*

$$\|\nabla w\|_{W_0^{2,p}(\Omega)} \leq \frac{C}{1-\beta_\sigma^{1/2}} \|g\|_{L^\infty(\Omega)}. \tag{2.14}$$

Remark 2.5. The constant α depends on Ω and β_σ, while C depends on $\lambda_{\min}(a)$ and, if $n \leq 4$, on $\|(\mathrm{tr}(\sigma))^{n/2-2-\epsilon}\|_{L^1(\Omega)}$.

PROOF: Now let us observe that

$$\frac{\nu_Q}{\det(\nabla F) \circ F^{-1}} = \frac{\mathrm{tr}(\sigma)}{\mathrm{tr}(\sigma^2)} \circ F^{-1}. \tag{2.15}$$

Using the change of variables $y = F(x)$ and choosing $1/q' + 1/q = 1$, we obtain that

$$\left\| \frac{\nu_Q}{\det(\nabla F) \circ F^{-1}} \hat{g} \right\|_{L^p(\Omega)} \leq \|g\|_{L^{pq'}(\Omega)} \left\| \frac{\mathrm{tr}(\sigma)}{\mathrm{tr}(\sigma^2)} (\det(\nabla F))^{1/pq} \right\|_{L^{pq}(\Omega)}. \tag{2.16}$$

It is easy to check that

$$\left\| \frac{\mathrm{tr}(\sigma)}{\mathrm{tr}(\sigma^2)} (\det(\nabla F))^{1/pq} \right\|_{L^{pq}(\Omega)}^{pq} \leq \frac{C_{qp,n}}{(\lambda_{\min}(a))^{n/2}} \int_\Omega (\mathrm{tr}(\sigma))^{n/2-qp}. \tag{2.17}$$

For $2 \leq n \leq 4$ we choose $q = 1$ in (2.17); for $n \geq 5$ we choose $q = n/2p$. Then a direct application of Theorem 2.1 and estimate (2.15) to equation (2.13) implies the theorem (observe that $\beta_Q = \beta_\sigma$). □

Let $\varphi \in C_0^\infty(\Omega)$. Write $\hat{\varphi} := \varphi \circ F^{-1}$. Using Theorem 2.4 we obtain that

$$\left(\hat{\varphi}, \sum_{i,j=1}^n Q_{ij} \partial_i \partial_j w \right)_{L^2(\Omega)} = -\left(\hat{\varphi}, \frac{\hat{g}}{|\det(\nabla F)| \circ F^{-1}} \right)_{L^2(\Omega)}. \tag{2.18}$$

Using the change of variable $y = F(x)$, we deduce that

$$\left(\varphi, \sum_{i,j=1}^n \sigma_{ij} (\partial_i \partial_j w) \circ F \right)_{L^2(\Omega)} = -(\varphi, g)_{L^2(\Omega)}. \tag{2.19}$$

Let us observe that

$$\sum_{i,j=1}^n \sigma_{ij} (\partial_i \partial_j w) \circ F = \mathrm{div}(a \nabla F((\nabla w) \circ F)). \tag{2.20}$$

After integrating by parts (and observing that $\nabla F (\nabla w) \circ F = \nabla (w \circ F)$), it follows that

$$a[\varphi, w \circ F] = (\varphi, g)_{L^2(\Omega)}. \tag{2.21}$$

It follows from the uniqueness of the solution of the Dirichlet problem (2.21) that $w \circ F = u$. Theorem 1.12 is then a straightforward consequence of Theorem 2.4 and the equality $u \circ F^{-1} = w$.

Remark 2.6. Using the change of variables $y = F(x)$, we obtain for all $\varphi \in C_0^\infty(\Omega)$

$$a[\varphi, u] = Q[\hat{\varphi}, \hat{u}]. \tag{2.22}$$

The comparison between (2.18) and (2.22) indicates that Q is a divergence-free matrix. We have not used that property of Q explicitly in our proof above, but it is present implicitly in the deduction of (2.21) from (2.20).

Remark 2.7. The only place where we use the convexity of Ω is for the validity of Lemma 2.3 (we refer to [57]).

The following lemma is a well-known result obtained from the De Giorgi–Moser–Nash theory [27, 59, 63] of divergence form elliptic operators with discontinuous coefficients (more precisely, we refer to [70] for global Hölder regularity).

LEMMA 2.8 *There exists $C, \alpha' > 0$ depending on Ω and $\lambda_{\max}(a)/\lambda_{\min}(a)$ such that F is α'-Hölder-continuous and*

$$\|F\|_{C^{\alpha'}} \leq C. \tag{2.23}$$

Theorem 1.4 is a straightforward consequence of the Sobolev embedding inequality (2.11), Theorem 2.4, Lemma 2.1, and the fact that $\nabla_F u = \nabla \hat{u} \circ F$. Let us observe that in dimension 2, we have

$$\frac{1}{1-\beta_\sigma} = \frac{1}{2}\left(\mu_\sigma + \frac{1}{\mu_\sigma}\right), \tag{2.24}$$

and the condition $\beta_\sigma < 1$ is equivalent to $\mu_\sigma < \infty$.

We will not assume Ω to be convex in Theorem 2.9 given below. Let $N^{p,\lambda}(\Omega)$ $(1 < p < \infty, 0 < \lambda < n)$ be the weighted Morrey space formed by functions $v : \Omega \to \mathbb{R}$ such that $\|v\|_{N^{p,\lambda}(\Omega)} < \infty$ with

$$\|v\|_{N^{p,\lambda}(\Omega)} = \sup_{x_0 \in \Omega} \left(\int_\Omega |x - x_0|^{-\lambda} |v(x)|^p \right)^{1/p}. \tag{2.25}$$

To obtain the Hölder continuity of $u \circ F^{-1}$ in dimension $n \geq 3$ we will use corollary 4.1 of [56]. We will give the result of S. Leonardi below in a form adapted to our context.

Consider the Dirichlet problem (2.2). We do not assume Ω to be bounded. We denote by $W^{2,p,\lambda}(\Omega)$ the functions in $W^{2,p}(\Omega)$ such that their second-order derivatives are in $N^{p,\lambda}(\omega)$.

THEOREM 2.9 *There exists a constant $C^* = C^*(n, p, \lambda, \partial\Omega) > 0$ such that if $\beta_M < C^*$ and $f \in N^{p,\lambda}(\Omega)$, then the Dirichlet problem* (2.2) *has a unique solution in $W^{2,p,\lambda} \cap W_0^{1,p}(\Omega)$. Moreover, if $0 < \lambda < n < p$, then $\nabla v \in C^\alpha(\Omega)$ with $\alpha = 1 - n/p$ and*

$$\|\nabla v\|_{C^\alpha(\Omega)} \leq \frac{C}{\lambda_{\min}(M)} \|f\|_{N^{p,\lambda}(\Omega)} \tag{2.26}$$

where $C = C(n, p, \lambda, \partial\Omega)$.

Theorem 1.14 is a straightforward application of Theorem 2.9.

2.2 Dimensionality Reduction

Let us prove Theorem 1.16. We denote by X_h the linear space spanned by the elements ψ_i. The solution of the Galerkin scheme satisfies $a[u - u_h, v] = 0$ for all $v \in X_h$. Thus

$$a[u - u_h] = \inf_{v \in X_h} a[u - u_h, u - v]. \tag{2.27}$$

It follows by the Cauchy-Schwarz inequality that

$$a[u - u_h] \leq \inf_{v \in X_h} a[u - v]. \tag{2.28}$$

Now writing $\hat{v} := v \circ F^{-1}$ and using the change of variable $y = F(x)$, we obtain

$$a[u - v] = Q[\hat{u} - \hat{v}]. \tag{2.29}$$

It follows in dimension $n = 2$ that

$$\|u - u_h\|_{H^1}^2 \leq \frac{D}{\lambda_{\min}(a)} \inf_{w \in V_h} \|\nabla \hat{u} - \nabla w\|_{L^\infty(\Omega)}^2 \tag{2.30}$$

with

$$D := \operatorname{tr}\left[\int_\Omega {}^{\mathsf{T}}\nabla F a \nabla F\right]. \tag{2.31}$$

Thus using the following standard approximation properties of the elements φ_i (see, for instance, [33]),

$$\inf_{w \in V_h} \|\nabla \hat{u} - \nabla w\|_{L^2(\Omega)} \leq C\gamma(\mathcal{T}_h) h^\alpha \|\hat{u}\|_{C_0^{1,\alpha}(\Omega)}, \tag{2.32}$$

we obtain that

$$\|u - u_h\|_{H^1} \leq \gamma(\mathcal{T}_h) \left(\frac{D}{\lambda_{\min}(a)}\right)^{1/2} \|\nabla \hat{u}\|_{C^\alpha} h^\alpha. \tag{2.33}$$

We conclude by observing that for $l \in \mathbb{R}^n$

$$\int_\Omega {}^{\mathsf{T}}l {}^{\mathsf{T}}\nabla F a \nabla F l = \inf_{f \in C_0^\infty(\Omega)} \int_\Omega {}^{\mathsf{T}}(l + \nabla f) a (l + \nabla f). \tag{2.34}$$

Theorem 1.16 becomes a direct consequence of (2.30) and Theorem 2.4.

In dimension $n \geq 3$ we obtain from (2.29) that

$$\|u - u_h\|_{H^1}^2 \leq \frac{\lambda_{\max}(Q)}{\lambda_{\min}(a)} \inf_{w \in V_h} \|\nabla \hat{u} - \nabla w\|_{L^2(\Omega)}^2. \tag{2.35}$$

It is easy to obtain that

$$\lambda_{\max}(Q) \leq (\det(a))^{1/2} \mu_\sigma^{n/2} (\operatorname{tr}(\sigma))^{1-n/2}. \tag{2.36}$$

We conclude by observing that $\mu_\sigma < C(\beta_\sigma)$ and using the following standard approximation properties of the elements φ_i (see, for instance, [33]):

$$\inf_{w\in V_h} \|\nabla\hat{u} - \nabla w\|_{L^2(\Omega)} \leq C\gamma(\mathcal{T}_h)h\|\hat{u}\|_{W_0^{2,2}(\Omega)}. \tag{2.37}$$

2.3 Galerkin with Localized Elements

Let us prove Theorem 1.27. We assume that the coarse mesh is not unadapted to F. Let K be a triangle of $\mathcal{T}_h$, and let a be a node of K such that $\eta^F_{\min}(K) = 1/\sin\theta$ where θ is the interior angle between $(F(a), F(b))$ and $(F(a), F(c))$, (b, c) being the other nodes of K. Let us prove the following lemma:

LEMMA 2.10

$$|\nabla_F u(K) - \nabla_F u(a)| \leq 3\eta^F_{\min}(K)\|\nabla\hat{u}\|_{C^\alpha}\|F\|^\alpha_{C^{\alpha'}}h^{\alpha\alpha'}. \tag{2.38}$$

PROOF: It is easy to check that

$$u(b) - u(a) = (F(b) - F(a))\nabla\hat{u}\circ F(a) + (F(b) - F(a))\cdot q_{ba}, \tag{2.39}$$

where the vector q_{ba} is defined by

$$q_{ba} := \int_0^1 [\nabla\hat{u}[F(a) + s(F(b) - F(a))] - \nabla\hat{u}[F(a)]]ds. \tag{2.40}$$

We will use the notation $f_{ba} := (F(b) - F(a))/|F(b) - F(a)|$. We will denote by $f_{ba}^\perp$ the unit vector obtained by a 90° rotation of f_{ba} toward f_{ca}. Defining q_{ca} as in (2.40), we obtain that

$$\nabla_F u(K) = \nabla_F u(a) + k \tag{2.41}$$

with

$$k = q_{ba} - \lambda f_{ba}^\perp \tag{2.42}$$

with

$$\lambda := \frac{f_{ca}\cdot(q_{ba} - q_{ca})}{f_{ca}\cdot f_{ba^\perp}}, \tag{2.43}$$

which leads us to

$$|\nabla_F u(K) - \nabla_F u(a)| \leq \frac{3}{f_{ca}\cdot f_{ba^\perp}}\|\nabla\hat{u}\|_{C^\alpha}\|F\|^\alpha_{C^{\alpha'}}h^{\alpha\alpha'}. \tag{2.44}$$

□

The following lemma is a direct consequence of Lemma 2.10:

LEMMA 2.11 *Let $K \in \mathcal{T}_h$ and let $x \in \Omega$; then*

$$|\nabla_F u(K) - \nabla_F u(x)| \leq 3\eta^*_{\min}\|\nabla\hat{u}\|_{C^\alpha}(1 + \|F\|^\alpha_{C^{\alpha'}})(h + \operatorname{dist}(x, K))^{\alpha\alpha'}. \tag{2.45}$$

Let us denote by $\mathcal{Z}_h u$ the interpolation of u over the space Z_h:

$$\mathcal{Z}_h u(x) = \sum_{i \in \mathcal{N}_h} u(x_i)\xi_i(x). \tag{2.46}$$

LEMMA 2.12 *We have*

$$a^*[u - \mathcal{Z}_h u] \leq C\eta^*_{\min} \|\nabla \hat{u}\|_{C^\alpha} \|F\|^\alpha_{C^{\alpha'}} h^{\alpha\alpha'} D. \tag{2.47}$$

PROOF: We have

$$a_K[u - \mathcal{Z}_h u] = \int_K {}^{\mathsf{T}}\big(\nabla_F u(x) - \nabla_F u(K)\big)\sigma(x)\big(\nabla_F u(x) - \nabla_F u(K)\big)dx \tag{2.48}$$

with $\sigma(x) := {}^{\mathsf{T}}\nabla F a \nabla F$. Using the change of variables $F(x) = y$, we obtain that

$$a_K[u - \mathcal{Z}_h u] = \int_{F(K)} {}^{\mathsf{T}}\big(\nabla \hat{u}(y) - \nabla_F u(K)\big)Q(y)\big(\nabla \hat{u}(y) - \nabla_F u(K)\big)dy, \tag{2.49}$$

from which we deduce that

$$a_K[u - \mathcal{Z}_h u] \leq (3\eta^*_{\min} \|\nabla \hat{u}\|_{C^\alpha} \|F\|^\alpha_{C^{\alpha'}} h^{\alpha\alpha'})^2 \int_{F(K)} \sup_{|e|=1} {}^{\mathsf{T}}eQe. \tag{2.50}$$

Thus,

$$a^*[u - \mathcal{Z}_h u] \leq C(\eta^*_{\min} \|\nabla \hat{u}\|_{C^\alpha} \|F\|^\alpha_{C^{\alpha'}} h^{\alpha\alpha'})^2 D \tag{2.51}$$

where D has been defined by (2.31). □

Theorem 1.27 is implied by Lemma 2.12, Theorem 2.4, Lemma 2.8, and the inequality

$$a^*[u - u^f] \leq a^*[u - \mathcal{Z}_h u]. \tag{2.52}$$

Let us now prove Theorem 1.31. By the triangle inequality

$$a[u - \mathcal{J}_h u^f] \leq a[u - \mathcal{J}_h u] + a[\mathcal{J}_h u - \mathcal{J}_h u^f]. \tag{2.53}$$

We write $\hat{\mathcal{J}}_h u := (\mathcal{J}_h u) \circ F^{-1}$. $\hat{\mathcal{J}}_h u$ is a linear interpolation of $\hat{u}$ on the tessellation $\mathcal{T}^F$. Now using the identity

$$a[u - \mathcal{J}_h u] = Q[\hat{u} - \hat{\mathcal{J}}_h u], \tag{2.54}$$

we obtain that

$$a[u - \mathcal{J}_h u] \leq \|\hat{u}\|_{C^\alpha} \hat{h}^\alpha D, \tag{2.55}$$

where we have denoted by $\hat{h}$ the maximal length of the edges of $\mathcal{T}^F$. Observe that $\hat{h} \leq h^{\alpha'} \|F\|_{C^{\alpha'}}$. Theorem 1.31 is a consequence of inequalities (2.53), (2.55), Lemmas 2.13 and 2.12, Theorem 2.4, and the inequality

$$a^*[\mathcal{Z}_h u - u^f] \leq 2a^*[u - \mathcal{Z}_h u].$$

LEMMA 2.13

$$a[\mathcal{J}_h u - \mathcal{J}_h u^f] \leq 2^6 \eta^*_{\max} \mu_\sigma^{1/2} \eta^3_{\max} \left(\frac{\lambda_{\max}(a)}{\lambda_{\min}(a)} \right)^{1/2} a^*[\mathcal{Z}_h u - u^f] \tag{2.56}$$

and

$$a[\mathcal{J}_h u - \mathcal{J}_h u^f] \leq \mu_\sigma \nu^* a^*[\mathcal{Z}_h u - u^f]. \tag{2.57}$$

PROOF: Let us write $w := \mathcal{J}_h u - \mathcal{J}_h u^f$. We need to bound $a[w]$. We have

$$a[w] = \frac{a^*[\mathcal{J}_h w]}{a^*[\mathcal{Z}_h w]} a^*[\mathcal{Z}_h w]. \tag{2.58}$$

The value of $a^*[\mathcal{Z}_h w] = a^*[\mathcal{Z}_h u - u^f]$ has already been estimated in Lemma 2.12. Observe that

$$a^*[\mathcal{J}_h w] = Q[\hat{w}]. \tag{2.59}$$

The function $\hat{w}$ is piecewise linear on $\mathcal{T}^F$. Using property (1.43), we obtain that

$$Q[\hat{w}] \leq \eta^*_{\max} \lambda_{\max}(Q) \mathcal{E}_h[w]. \tag{2.60}$$

Moreover, observing that

$$Q \circ F = \frac{\sigma}{(\det(\sigma))^{1/2}} (\det(a))^{1/2}, \tag{2.61}$$

we obtain that

$$\lambda_{\max}(Q) \leq \mu_\sigma^{1/2} (\det(a))^{1/2}. \tag{2.62}$$

Equation (2.62) is valid in dimension 2; in dimension higher than 2 we would use the inequality (2.36)

$$\lambda_{\max}(Q) \leq \mu_\sigma^{1/2} (\lambda_{\min}(\sigma))^{(n-2)/2} (\det(a))^{1/2}. \tag{2.63}$$

We now need to bound from below $a^*[\mathcal{Z}_h w]/\mathcal{E}_h[w]$. For $K \in \mathcal{T}_h$ let us denote by $H(K)$ the matrix

$$H(K) := \int_K {}^{\mathsf{T}}(\nabla F(K))^{-1\mathsf{T}} \nabla F(x) a \nabla F(x) (\nabla F(K))^{-1} \, dx. \tag{2.64}$$

We need to estimate $\inf_{|l|=1} {}^{\mathsf{T}} l H(K) l$. Let us denote by a, b, and c the nodes of K and

$$f(x) := (F(x) - F(a))(\nabla F(K))^{-1} \cdot l. \tag{2.65}$$

Let us observe that

$$ {}^{\mathsf{T}} l H(K) l = \int_K {}^{\mathsf{T}} \nabla f a \nabla f. \tag{2.66}$$

Moreover, $f(a) = 0$, $f(b) = (b-a)\cdot l$, and $f(c) = (c-a)\cdot l$. Let us assume without loss of generality that $|f(b)|/|b-a| \geq |f(c)|/|c-a|$. Then

$$ {}^{\mathsf{T}}lH(K)l \geq \inf_{\substack{w\in C^{\infty}(\Omega)\\ w(a)=0\\ w(b)=f(b)}} \int_K {}^{\mathsf{T}}\nabla w a \nabla w. \tag{2.67} $$

The quantity appearing in (2.67) is the resistance metric distance between the points a and b, and it is easy to check that (see, for instance, lemma 1.1 of [8])

$$ \inf_{\substack{w\in C^{\infty}(\Omega)\\ w(a)=0\\ w(b)=f(b)}} \int_K {}^{\mathsf{T}}\nabla w a \nabla w \geq \lambda_{\min}(a)\,\mathrm{vol}(K)\left(\frac{|f(b)|}{|b-a|}\right)^2. \tag{2.68} $$

Thus

$$ {}^{\mathsf{T}}lH(K)l \geq \lambda_{\min}(a)\,\mathrm{vol}(K)\left(\frac{|(b-a)\cdot l|}{|b-a|}\right)^2. \tag{2.69} $$

Let us observe that

$$ \frac{|(b-a)\cdot l|}{|b-a|} \geq \frac{1}{4\eta_{\max}}. \tag{2.70} $$

It follows that

$$ a^*[\mathcal{Z}_h w] \geq \|\nabla \mathcal{I}_h w\|^2_{L^2}\lambda_{\min}(a)\frac{1}{16\eta^2_{\max}}. \tag{2.71} $$

Thus

$$ \frac{a^*[\mathcal{Z}_h w]}{\mathcal{E}_h[w]} \geq \lambda_{\min}(a)\frac{1}{2^6\eta^3_{\max}}, \tag{2.72} $$

which leads us to equation (2.56).

Remark 2.14. One of the methods employed with nonconformal elements to ensure the stability and convergence of the scheme is the so-called patch test. In our proof the stability condition and convergence are ensured by (2.72) and a uniform lower bound on $\eta_{\max}$.

To obtain (2.57), let us observe that

$$ a[w] = Q[\hat{w}]. \tag{2.73} $$

Thus

$$ a[w] = \sum_{K\in\mathcal{T}_h}\int_{K^F} {}^{\mathsf{T}}\nabla\hat{w}(K^F)Q(y)\nabla\hat{w}(K^F)dy. \tag{2.74} $$

It follows that

$$ a[w] \leq \nu^* \sum_{K\in\mathcal{T}_h}\int_{F(K)} \frac{\lambda_{\max}(Q)}{\lambda_{\min}(Q)} {}^{\mathsf{T}}\nabla\hat{w}(K^F)Q(y)\nabla\hat{w}(K^F)dy. \tag{2.75} $$

From equation (2.61) we obtain that

$$\frac{\lambda_{\max}(Q)}{\lambda_{\min}(Q)} \leq \mu_\sigma. \tag{2.76}$$

Next, observing that

$$\sum_{K\in\mathcal{T}_h} \int_{F(K)} {}^{\mathsf{T}}\nabla\hat{w}(K^F)Q(y)\nabla\hat{w}(K^F)dy = a^*[\mathcal{Z}_h w], \tag{2.77}$$

we obtain (2.57). □

2.4 Numerical Homogenization from the Information Point of View

In this section we will prove Theorem 1.36 and Theorem 1.38. The method introduced in Section 1.4 can be formulated in the following way: look for $u^m \in V_h$ such that for all $i \in \mathcal{N}_h$,

$$a^*[\varphi_i, \mathcal{Z}_h u^m] = (\varphi_i, g)_{L^2\Omega}, \tag{2.78}$$

which implies the following finite-volume orthogonality property for all $i \in \mathcal{N}_h$:

$$a^*[\varphi_i, \mathcal{Z}_h u^m - u] = 0. \tag{2.79}$$

Let us write $w = u - \mathcal{Z}_h u^m$. By equation (1.42) we obtain that

$$(\mathcal{E}_h[w])^{1/2} \leq \frac{1}{S^m} \sup_{v\in Z_h} \frac{a^*[v, \mathcal{Z}_h w]}{(\mathcal{E}_h[v])^{1/2}}. \tag{2.80}$$

By the orthogonality property, we have

$$a^*[v, \mathcal{Z}_h w] = a^*[v, \mathcal{Z}_h u - u]. \tag{2.81}$$

Thus

$$a^*[v, \mathcal{Z}_h w] \leq (\lambda_{\max}(a))^{1/2}\|\nabla v\|_{L^2(\Omega)}(a^*[\mathcal{Z}_h u - u])^{1/2}. \tag{2.82}$$

Using the inequality

$$\|\nabla v\|^2_{L^2(\Omega)} \leq \eta_{\max}\mathcal{E}_h[v], \tag{2.83}$$

we deduce that

$$\mathcal{E}_h[w]^{1/2} \leq \frac{1}{S^m}(\lambda_{\max}(a)\eta_{\max})^{1/2}(a^*[\mathcal{Z}_h u - u])^{1/2}. \tag{2.84}$$

It follows from (1.43) that

$$\|\nabla\mathcal{I}_h u - \nabla u^m\|_{L^2(\Omega)} \leq \frac{\eta_{\max}}{S^m}(\lambda_{\max}(a))^{1/2}(a^*[\mathcal{Z}_h u - u])^{1/2}, \tag{2.85}$$

and we deduce from the Poincaré inequality that

$$\|\mathcal{I}_h u - u^m\|_{L^2(\Omega)} \leq C_\Omega \frac{\eta_{\max}}{S^m}(\lambda_{\max}(a))^{1/2}(a^*[\mathcal{Z}_h u - u])^{1/2}. \tag{2.86}$$

We obtain Theorem 1.36 from equations (2.85) and (2.86), Lemma 2.12, and Theorem 2.4.

Let us now prove Theorem 1.38. Using the triangle inequality, we obtain

$$a[u - \mathcal{J}_h u^m] \leq a[u - \mathcal{J}_h u] + a[\mathcal{J}_h u - \mathcal{J}_h u^m]. \tag{2.87}$$

The object $a[u - \mathcal{J}_h u]$ has already been bounded from above by (2.55). Writing $w := \mathcal{J}_h u - \mathcal{J}_h u^m$, we have

$$a[w] = \frac{a[\mathcal{J}_h w]}{\mathcal{E}_h[w]}\, \mathcal{E}_h[w]. \tag{2.88}$$

But $\mathcal{E}_h[w]$ has already been estimated in equation (2.84). It remains to notice that

$$a[\mathcal{J}_h w] = Q[\hat{w}]. \tag{2.89}$$

From this point the arguments are similar to the ones employed in Section 2.3; indeed,

$$Q[\hat{w}] \leq \lambda_{\max}(Q) \|\nabla \hat{w}\|_{L^2(\Omega)} \leq \eta^*_{\max} \lambda_{\max}(Q) \mathcal{E}_h[w]. \tag{2.90}$$

2.5 Numerical Homogenization from a Transport Point of View

We assume the mesh to be regular in the following sense: the nodes of the Vornoï diagram of $\mathcal{T}_h$ are contained in the triangles of the primal mesh $\mathcal{T}_h$. In dimension 2 this means that for each triangle $K \in \mathcal{T}_h$ the intersection of the median of K (the circumcenter) belongs to the interior of K. Let us denote by Y_h the vector space spanned by the functions χ_i. For $v \in Z_h$ we define $\mathcal{Y}_h v$ by

$$\mathcal{Y}_h v := \sum_{i \in \mathcal{N}_h} v_i \chi_i. \tag{2.91}$$

The metric numerical homogenization method can be formulated in the following way: look for $u^v \in Z_h$ (the space spanned by the elements ξ_i) such that for all $i \in \mathcal{N}_h$,

$$a^*[\chi_i, u^v] = (\chi_i, g)_{L^2\Omega}, \tag{2.92}$$

which implies the following finite-volume orthogonality property for all $i \in \mathcal{N}_h$,

$$a^*[\chi_i, u^v - u] = 0. \tag{2.93}$$

Equation (2.92) can be written as

$$\sum_{j \sim i} u_j^v \int_{\partial V_i} n \cdot a \cdot \nabla \xi_i = \int_{V_i} g. \tag{2.94}$$

Let us write $w := \mathcal{Z}_h u - u^v$. From equation (1.58) we obtain that

$$(\mathcal{E}_h[w])^{1/2} \leq \frac{1}{\mathcal{S}^v} \sup_{v \in \mathcal{Y}_h} \frac{a^*[v, w]}{(\mathcal{E}_h[v])^{1/2}}. \tag{2.95}$$

Using the orthogonality property of the finite-volume method, we obtain that for $v \in \mathcal{Y}_h$

$$a^*[v, w] = -\sum_{i \in \mathcal{N}_h} v_i \int_{\partial V_i} n \cdot a(\nabla \mathcal{Z}_h u - \nabla u). \tag{2.96}$$

Denoting by $\mathcal{E}_h^*$ the edges of the dual tessellation (edges of the control volumes), we obtain that

$$a^*[v, w] = \sum_{e_{ij} \in \mathcal{E}_h^*} (v_j - v_i) \int_{e_{ij}} n_{ij} \cdot a(\nabla \mathcal{Z}_h u - \nabla u), \tag{2.97}$$

where e_{ij} is the edge separating the control volume V_i from the control volume V_j and n_{ij} is the unit vector orthogonal to e_{ij} pointing outside of V_i. It follows that

$$\begin{aligned} a^*[v, w] \leq (\mathcal{E}_h[v])^{1/2} &\|\nabla_F \mathcal{Z}_h u - \nabla_F u\|_{L^\infty(\mathcal{E}_h^*)} \\ &\cdot \left(\sum_{e_{ij} \in \mathcal{E}_h^*} |e_{ij}|^2 \lambda_{\max}(a) \lambda_{\max}(\sigma) \right)^{1/2}. \end{aligned} \tag{2.98}$$

Now let us observe that

$$\sum_{e_{ij} \in \mathcal{E}_h^*} |e_{ij}|^2 \leq 3\eta_{\max} \operatorname{vol}(\Omega). \tag{2.99}$$

We then have from equation (2.95)

$$\begin{aligned} (\mathcal{E}_h[w])^{1/2} \leq \frac{3}{\mathcal{S}^v} &\|\nabla_F \mathcal{Z}_h u - \nabla_F u\|_{L^\infty(\mathcal{E}_h^*)} \\ &\cdot \eta_{\max} \operatorname{vol}(\Omega) (\lambda_{\max}(a) \lambda_{\max}(\sigma))^{1/2}. \end{aligned} \tag{2.100}$$

Equation (1.59) of Theorem 1.40 is then a straightforward consequence of equation (1.43) and Lemma 2.11.

Let us now prove equation (1.60) of Theorem 1.40. By the triangle inequality

$$a[u - \mathcal{J}_h u^v] \leq a[u - \mathcal{J}_h u] + a[\mathcal{J}_h u - \mathcal{J}_h u^v]. \tag{2.101}$$

$a[u - \mathcal{J}_h u]$ has already been estimated in equation (2.55). Writing $w := \mathcal{J}_h u - \mathcal{J}_h u^v$ we have

$$a[w] = \frac{a^*[\mathcal{J}_h w]}{\mathcal{E}_h[w]} \mathcal{E}_h[w]. \tag{2.102}$$

But $\mathcal{E}_h[w]$ has already been estimated in equation (2.100). It remains to note that $a^*[\mathcal{J}_h w]/\mathcal{E}_h[w]$ has already been estimated in equations (2.59) and (2.60), thus concluding the proof.

3 Numerical Experiments

Let us now illustrate the implementation of this method. The domain is the unit disk in dimension 2. Equation (1.1) is solved on a fine tessellation characterized by 66 049 nodes and 131 072 triangles. The coarse tessellation has 289 nodes and 512 triangles (Figure 3.1). It is important to recall that since our methods involve the computation of global harmonic coordinates, the memory requirement and CPU time are not improved if one needs to solve (1.1) only one time, whereas localized methods such as the one of Hou and Wu or E and Engquist do improve the memory requirement or the CPU time.

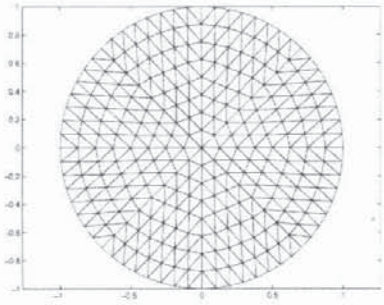

FIGURE 3.1. Coarse grid.

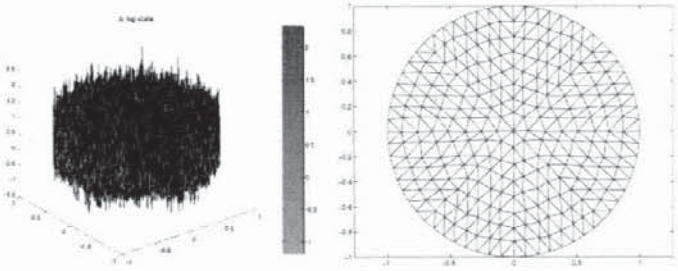

(a) a. **(b)** $\mathcal{T}^F$.

FIGURE 3.2. Example 1, trigonometric multiscale.

The elliptic operator associated to equation (1.1) has been upscaled to an operator defined on the coarse mesh (compression by a factor of 300) using five different methods:

- the Galerkin scheme described in Section 1.2 using the multiscale finite element ψ_i, denoted FEM_ψ,
- the Galerkin scheme described in Section 1.3 using the localized elements ξ_i, denoted FEM_ξ,
- the metric-based compression scheme described in Section 1.4, denoted MBFEM,
- the finite-volume method described in Section 1.5, denoted FVM,
- a multiscale finite element method, denoted LFEM, where F is computed locally (instead of globally) on each triangle K of the coarse mesh as the solution of a cell problem with boundary condition $F(x) = x$ on ∂K. This method has been implemented in order to understand the effect of the removal of global information on the structure of the metric induced by F.

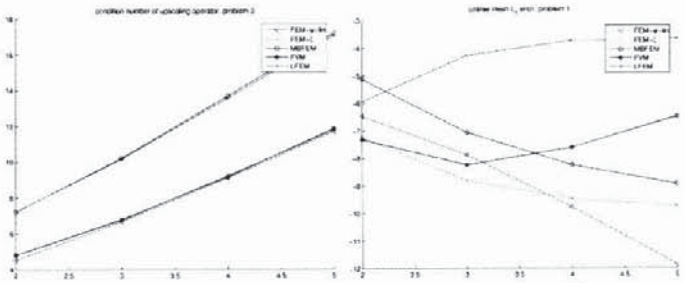

(a) Condition number. (b) Coarse-mesh L^1 error.

FIGURE 3.3. Example 1, trigonometric multiscale.

Example 1 (Trigonometric Multiscale).

$$a(x) = \frac{1}{6}\left(\frac{1.1+\sin(2\pi x/\epsilon_1)}{1.1+\sin(2\pi y/\epsilon_1)} + \frac{1.1+\sin(2\pi y/\epsilon_2)}{1.1+\cos(2\pi x/\epsilon_2)} + \frac{1.1+\cos(2\pi x/\epsilon_3)}{1.1+\sin(2\pi y/\epsilon_3)} + \frac{1.1+\sin(2\pi y/\epsilon_4)}{1.1+\cos(2\pi x/\epsilon_4)} + \frac{1.1+\cos(2\pi x/\epsilon_5)}{1.1+\sin(2\pi y/\epsilon_5)} + \sin(4x^2y^2) + 1\right),$$

where

$$\epsilon_1 = \frac{1}{5}, \quad \epsilon_2 = \frac{1}{13}, \quad \epsilon_3 = \frac{1}{17}, \quad \epsilon_4 = \frac{1}{31}, \quad \epsilon_5 = \frac{1}{65}.$$

Figure 3.2 is an illustration of $\mathcal{T}^F$, the deformation of the coarse mesh (Figure 3.1) under the metric induced by F. The deformation is small since the medium is quasi-periodic. The weak aspect ratio for triangles the coarse mesh in the metric induced by F (defined by equation (1.20)) is $\eta^*_{\min} = 1.1252$.

Table 3.1 gives the relative error estimated on the nodes of the coarse mesh between the solution u of the initial PDE (1.1) and an approximation obtained from the upscaled operator on the nodes of the coarse mesh. Table 3.2 gives the relative error estimated on the nodes of the fine mesh between u and the $\mathcal{J}_h$-interpolation of the previous approximations with respect to F on a fine resolution. Figure 3.3(a) gives the condition number of the stiffness matrix associated to the upscaled operator versus $-\log_2 h$ (logarithm of the resolution). Figure 3.3(b) gives the relative L_1-distance between u and its approximation on the coarse mesh in log scale versus $-\log_2 h$ (logarithm of the resolution).

Observe that for the LFEM method, this error increase with the resolution is an effect of the so-called cell resonance observed in [2, 51]. This cell resonance does not occur with the methods proposed in this paper. The finite-volume method is characterized by the the best stability and one of the most accurate at a coarse resolution. The increase in the error observed for this method as the resolution is decreased is a numerical artifact created by the fine mesh: one has to divide the

Coarse mesh error	FEM_ψ	FEM_ξ	MBFEM	FVM	LFEM
L^1	0.0042	0.0022	0.0075	0.0032	0.0411
L^2	0.0039	0.0024	0.0074	0.0040	0.0441
L^∞	0.0059	0.0090	0.0154	0.0117	0.0496
H^1	0.0060	0.0262	0.0568	0.0203	0.0763

TABLE 3.1. Example 1, trigonometric multiscale, coarse mesh error.

Fine mesh error	FEM_ψ	FEM_ξ	MBFEM	FVM	LFEM
L^1	0.0042	0.0085	0.0053	0.0080	0.0593
L^2	0.0043	0.0082	0.0061	0.0078	0.0591
L^∞	0.0063	0.0112	0.0154	0.0141	0.0597
H^1	0.0581	0.0540	0.0778	0.0601	0.0943

TABLE 3.2. Example 1, trigononmetric multiscale, fine mesh error.

coarse tessellation into coarse control volumes. These coarse control volumes are unions of the control volumes defined on a fine mesh, and when the refinement between the coarse and the fine mesh is small and the triangulation irregular, it is not possible to divide the coarse tessellation into control volumes intersecting the edges of the primal mesh close to the midpoints of those edges and the other control volumes close to the barycenters of the coarse triangles.

Example 2 (High-Conductivity Channel). In this example a is random and characterized by a fine and long-ranged high-conductivity channel. We choose $a(x) = 100$ if x is in the channel and $a(x) = O(1)$ if x is not in the channel. The weak aspect ratio of the triangles of the coarse mesh in the metric induced by F is $\eta^\star_{\min} = 2.2630$. Table 3.3 gives the relative error estimated on the nodes of the coarse mesh between the solution u of the initial PDE (1.1) and an approximation obtained from the upscaled operator on the nodes of the coarse mesh. Table 3.4 gives the relative error estimated on the nodes of the fine mesh between u and the $\mathcal{J}_h$-interpolation of the previous approximations with respect to F on a fine resolution. Figure 3.5(a) gives the condition number of the stiffness matrix associated to the upscaled operator versus $-\log_2 h$ (logarithm of the resolution). Figure 3.5(b) gives the relative L_1-distance between u and its approximation on the coarse mesh in log scale versus $-\log_2 h$.

Observe in Figure 3.4 that the effect of the new metric on the mesh is to bring close together nodes linked by a path of low electrical resistance.

Remark 3.1. Let us recall that the natural distance associated to the Laplace operator on a fractal space is also the so-called resistance metric [8, 55, 71]. It is thus natural to find that a similar (not equivalent) notion of distance allows the

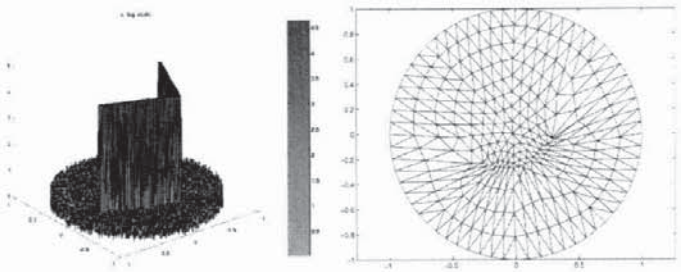

(a) a. (b) $\mathcal{T}^F$.

FIGURE 3.4. Example 2, high-conductivity channel.

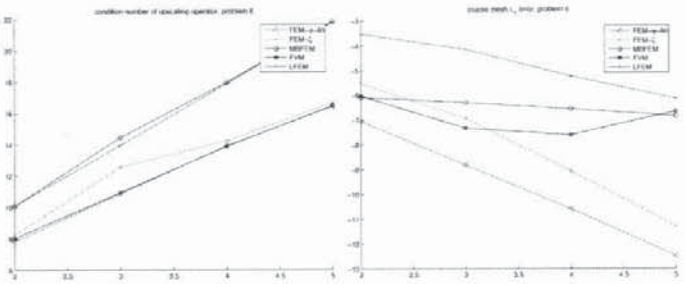

(a) Condition number. (b) Coarse-mesh L^1 error.

FIGURE 3.5. Example 2, high-conductivity channel error plots.

Coarse mesh error	FEM_ψ	FEM_ξ	MBFEM	FVM	LFEM
L^1	0.0022	0.0081	0.0127	0.0062	0.0519
L^2	0.0025	0.0096	0.0179	0.0081	0.0606
L^∞	0.0120	0.0227	0.0549	0.0174	0.1223
H^1	0.0120	0.0384	0.0919	0.0265	0.1514

TABLE 3.3. Example 2, high-conductivity channel, coarse mesh error.

numerical homogenization PDEs with arbitrary coefficients. More precisely, the analogues of the resistance metric here are the harmonic mappings. The analysis of these mappings allows us to bypass boundary layer effects in homogenization in periodic media [2] and to obtain quantitative estimates on the heat kernel of periodic operators [65] or to analyze PDEs characterized by an infinite number of nonseparated scales [14, 66].

Fine mesh error	FEM_ψ	FEM_ξ	MBFEM	FVM	LFEM
L^1	0.0070	0.0155	0.0164	0.0121	0.0612
L^2	0.0069	0.0153	0.0202	0.0123	0.0743
L^∞	0.0133	0.0227	0.0573	0.0214	0.1226
H^1	0.0760	0.1032	0.1838	0.0820	0.2142

TABLE 3.4. Example 2, high-conductivity channel, fine mesh error.

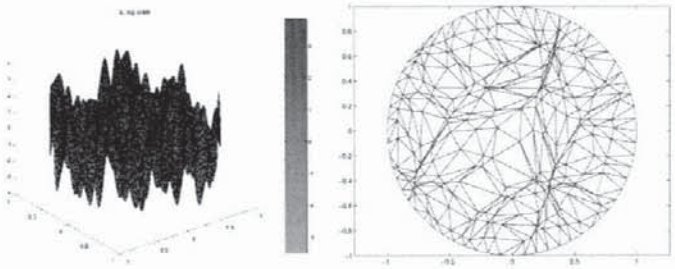

(a) a. **(b)** $\mathcal{T}^F$.

FIGURE 3.6. Example 3, random Fourier modes.

Example 3 (Random Fourier Modes). In this case, $a(x) = e^{h(x)}$, with

$$h(x) = \sum_{|k|\leq R} \left(a_k \sin(2\pi k \cdot x) + b_k \cos(2\pi k \cdot x)\right)$$

where a_k and b_k are independent identically distributed random variables on $[-0.3, 0.3]$ and $R = 6$. This is another example where scales are not separated. The weak aspect ratio of the triangles in the metric induced by F is $\eta^\star_{\min} = 3.4997$. Observe the deformation induced by the new metric (Figure 3.6). Observe that distances between u and the interpolation of the coarse-mesh approximations to the fine mesh are larger (Tables 3.5 and 3.6); this is due to the fact that those errors depend on the aspect ratio $\eta^*_{\max}$ (which is not the case for the coarse-mesh errors). Of course, one could improve the compression by adapting the mesh to the new metric, but this has not been our point of view here. We have preferred to show raw data obtained with a given coarse mesh. Figures 3.8 and 3.9 give the L^1, L^2, L^∞, and H^1 relative error ($\log_2$ basis versus $\log_2$ basis of the resolution). The x-axis corresponds to the refinement of coarse mesh; the y-axis is the error. Tables 3.7 and 3.8 give the convergence rate in different norms (the parameter α in the error of the order of h^α).

Example 4 (Random Fractal). In this case, a is given by a product of discontinuous functions oscillating randomly at different scales, $a(x) = a_1(x)a_2(x)\cdots a_n(x)$, and $a_i(x) = c_{pq}$ for $x \in [p/2^i, (p+1)/2^i) \times [q/2^i, (q+1)/2^i)$, c_{pq} is uniformly random in $[1/\gamma, \gamma]$, $n = 5$, and $\gamma = 2$. The weak aspect ratio is $\eta^\star_{\min} = 2.4796$.

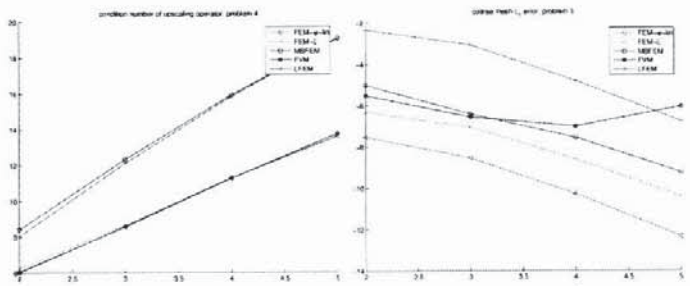

(a) Condition number. (b) Coarse mesh L^1 error.

FIGURE 3.7. Example 3, random Fourier modes error plots.

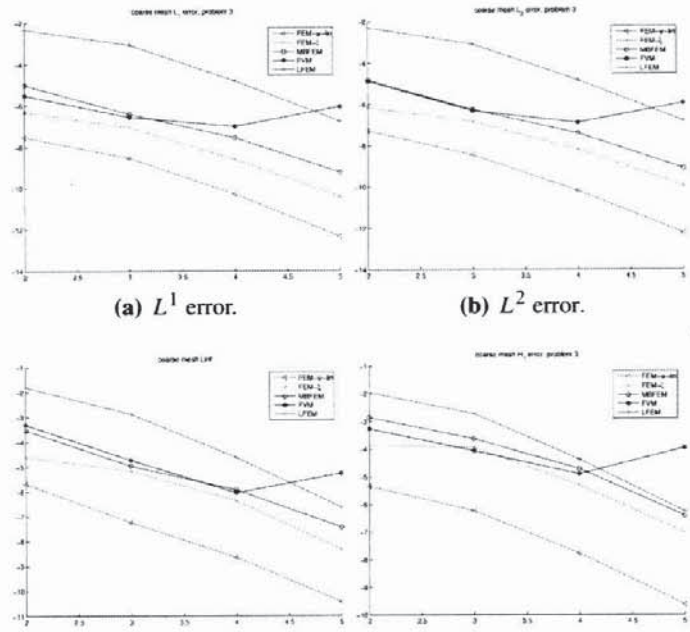

(a) L^1 error. (b) L^2 error.

(c) L^∞ error. (d) H^1 error.

FIGURE 3.8. Coarse-mesh error ($\log_2$): L^1, L^2, L^∞, and H^1 errors versus coarse-mesh refinement, Example 3, random Fourier modes.

Table 3.9 gives the relative error estimated on the nodes of the coarse mesh between the solution u of the initial PDE (1.1) and an approximation obtained from the upscaled operator on the nodes of the coarse mesh. Table 3.10 gives the relative error estimated on the nodes of the fine mesh between u and the $\mathcal{J}_h$-interpolation of the previous approximations with respect to F on a fine resolution. Figure 3.11(a) gives the condition number of the stiffness matrix associated to the upscaled operator versus $-\log_2 h$ (logarithm of the resolution). Figure 3.11(b) gives the relative

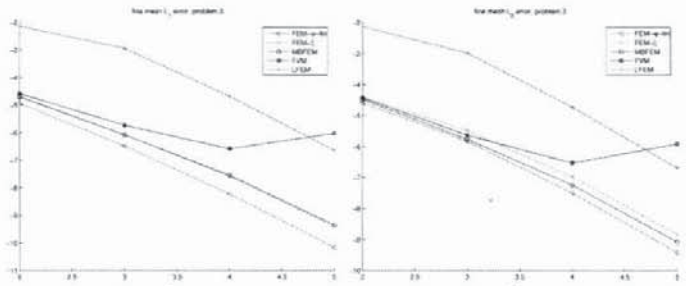

(a) L^1 error. (b) L^2 error.

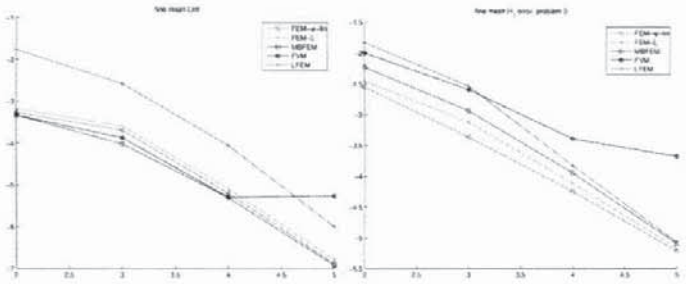

(c) L^∞ error. (d) H^1 error.

FIGURE 3.9. Fine-mesh approximation error ($\log_2$): L^1, L^2, L^∞, and H^1 errors versus coarse-mesh refinement for Example 3, random Fourier modes.

Coarse mesh error	FEM_ψ	FEM_ξ	MBFEM	FVM	LFEM
L^1	0.0027	0.0075	0.0117	0.0106	0.1197
L^2	0.0028	0.0087	0.0130	0.0125	0.1169
L^∞	0.0066	0.0278	0.0320	0.0376	0.1358
H^1	0.0133	0.0648	0.0805	0.0597	0.1514

TABLE 3.5. Example 3, random Fourier modes, coarse mesh error.

L_1-distance between u and its approximation on the coarse mesh in log scale versus $-\log_2 h$.

Example 5 (Percolation at Criticality). In this case, the conductivity of each site is equal to γ or $1/\gamma$ with probability $\frac{1}{2}$. We have chosen $\gamma = 4$ in this example. Observe that some errors are larger for this challenging case because a percolating medium generates flat triangles in the new metric; indeed, $\eta^\star_{\min} = 22.3395$. Table 3.11 gives the relative error estimated on the nodes of the coarse mesh between the solution u of the initial PDE (1.1) and an approximation obtained from the upscaled operator on the nodes of the coarse mesh. Table 3.12 gives the relative error estimated on the nodes of the fine mesh between u and the $\mathcal{J}_h$-interpolation of

Fine mesh error	FEM_ψ	FEM_ξ	MBFEM	FVM	LFEM
L^1	0.0112	0.0148	0.0148	0.0188	0.1304
L^2	0.0177	0.0223	0.0184	0.0202	0.1265
L^∞	0.0773	0.0824	0.0614	0.0680	0.1669
H^1	0.0972	0.1152	0.1307	0.1659	0.1725

TABLE 3.6. Example 3, random Fourier modes, fine mesh error.

Method	L^1	L^2	L^∞	H^1
FEM_ψ	1.62	1.66	1.56	1.44
FEM_ξ	1.38	1.27	1.23	1.18
MBFEM	1.38	1.40	1.27	1.08
FVM	0.53	1.14	1.26	1.03
LFEM	1.51	1.53	1.62	1.46

TABLE 3.7. Coarse-mesh approximation convergence rate.

Method	L^1	L^2	L^∞	H^1
FEM_ψ	1.74	1.61	1.23	0.89
FEM_ξ	1.57	1.47	1.23	0.91
MBFEM	1.54	1.52	1.21	0.96
FVM	0.75	1.16	1.22	0.58
LFEM	1.52	1.54	1.42	1.10

TABLE 3.8. Fine-mesh approximation convergence rate.

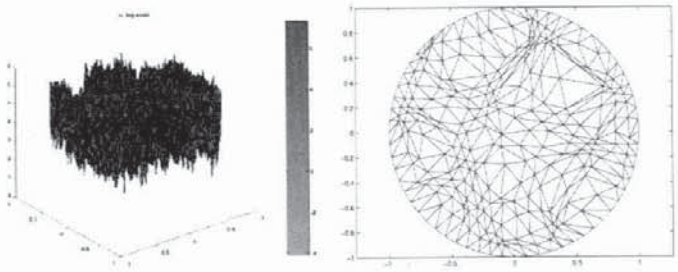

(a) a. **(b)** $\mathcal{T}^F$.

FIGURE 3.10. Example 4, random fractal.

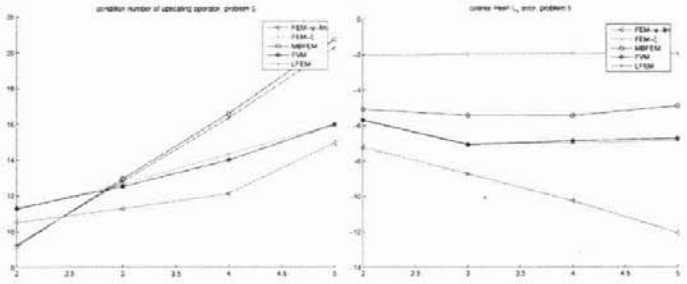

(a) Condition number. (b) Coarse-mesh L^1 error.

FIGURE 3.11. Example 4, random fractal error plots.

Coarse mesh error	FEM_ψ	FEM_ξ	MBFEM	FVM	LFEM
L^1	0.0024	0.0075	0.0231	0.0073	0.0519
L^2	0.0025	0.0085	0.0241	0.0100	0.0606
L^∞	0.0094	0.0399	0.0920	0.0398	0.1694
H^1	0.0161	0.0718	0.1553	0.0493	0.3107

TABLE 3.9. Example 4, random fractal, coarse mesh error.

Fine mesh error	FEM_ψ	FEM_ξ	MBFEM	FVM	LFEM
L^1	0.0108	0.0147	0.0245	0.0142	0.0765
L^2	0.0155	0.0198	0.0280	0.0173	0.0812
L^∞	0.0662	0.0802	0.0919	0.0720	0.1694
H^1	0.1015	0.1231	0.1838	0.1433	0.2642

TABLE 3.10. Example 4, random fractal, fine mesh error.

the previous approximations with respect to F on a fine resolution. Figure 3.13(a) gives the condition number of the stiffness matrix associated to the upscaled operator versus $-\log_2 h$ (logarithm of the resolution). Figure 3.13(b) gives the relative L_1-distance between u and its approximation on the coarse mesh in log scale versus $-\log_2 h$. Observe that the methods based on a global change of metric do converge, but when that numerical homogenization is done by computing only local coarse parameters (in averaging or finite element techniques), then convergence is not guaranteed without further assumptions on a (see the curve of LFEM).

3.1 Numerical Experiments with Splines

We have seen that if σ is stable, then $u \circ F^{-1}$ belongs to $W^{2,p}(\Omega)$ with $p > 2$. It is thus natural to expect a better accuracy by using C^1-continuous elements in the

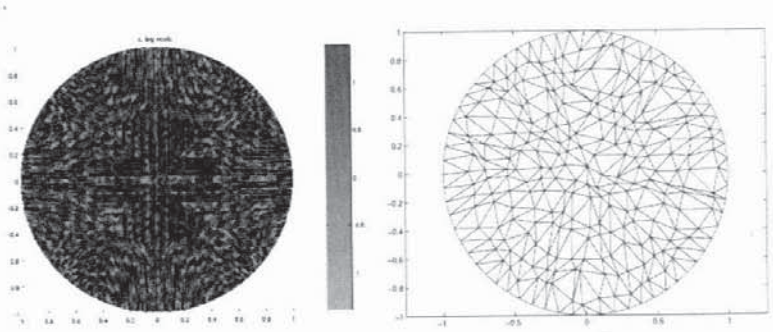

(a) a. (b) $\mathcal{T}^F$.

FIGURE 3.12. Example 5, percolation.

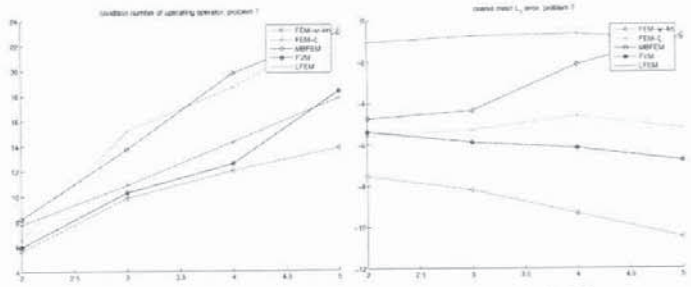

(a) Condition number. (b) Coarse-mesh L^1 error.

FIGURE 3.13. Example 5, percolation error plots.

Coarse mesh error	FEM_ψ	FEM_ξ	MBFEM	FVM	LFEM
L^1	0.0034	0.0253	0.0485	0.0167	0.2848
L^2	0.0041	0.0265	0.0523	0.0189	0.2851
L^∞	0.0163	0.0813	0.0643	0.0499	0.3018
H^1	0.0343	0.0843	0.1070	0.0713	0.3740

TABLE 3.11. Example 5, percolation, coarse mesh error.

method described in Section 1.2 instead of piecewise linear elements. This increase in accuracy has already been observed in [2] when F is obtained as the solution of a local cell problem. In our case (the harmonic coordinates are computed globally) we also observe a sharp increase in the accuracy of the finite element method of Section 1.2 by using splines for the elements φ_i.

We refer to [24, 49] for methods using C^1 finite elements. One possibility is the weighted extended B-splines (WEB) method developed by K. Höllig in [48, 49];

Fine mesh error	FEM_ψ	FEM_ξ	MBFEM	FVM	LFEM
L^1	0.0115	0.0265	0.0585	0.0216	0.3024
L^2	0.0152	0.0268	0.0628	0.0229	0.3015
L^∞	0.0500	0.0527	0.0940	0.0497	0.3135
H^1	0.1000	0.1712	0.1954	0.1343	0.3964

TABLE 3.12. Example 5, percolation, fine mesh error.

these elements are C^2-continuous. They are obtained from tensor products of one-dimensional elements. The Dirichlet boundary condition is satisfied using a smooth weight function ω such that $\omega = 0$ at the boundary. The condition number of the stiffness matrix is bounded from above by $O(h^{-2})$ (we have the same optimal bound on a Galerkin system with piecewise linear elements).

We have considered two challenging multiscale media for our numerical experiments: random Fourier modes and percolation. For the simplicity of the implementation, a square domain has been considered, and a weighted spline basis is used instead of the WEB spline basis. For a square domain $[-1, 1] \times [-1, 1]$, the weight is $\omega = (1 - x^2)(1 - y^2)$. Two methods have been compared:

- the Galerkin scheme using the finite elements $\psi_i = \varphi_i \circ F$, where φ_i are the piecewise linear nodal basis elements of Section 1.2, denoted by FEM_ψ_{lin}, and
- the Galerkin scheme using the finite element $\psi_i = \phi_i \circ F$, where ϕ_i are weighted cubic B-spline basis elements, denoted by FEM_ψ_{sp}.

The error obtained with the FEM_ψ_{sp} method is much smaller than that obtained with the FEM_ψ_{lin} method, as shown in Figures 3.14 and 3.15.

Acknowledgments. Part of the work of the first author has been supported by Le Centre National de la Recherche Scientifique (CNRS). The authors would like to thank Jean-Michel Roquejoffre for pointing out to us the correct references on nonlinear PDEs, Mathieu Desbrun for enlightening discussions on discrete exterior calculus [58] (a powerful tool that has shown the intrinsic way to define discrete differential operators on irregular triangulations), Tom Hou and Jerry Marsden for stimulating discussions on multiscale computation, and Clothilde Melot and Stéphane Jaffard for stimulating discussions on multifractal analysis. Thanks are also due to Lexing Ying and Laurent Demanet for useful comments on the manuscript and G. Ben Arous for introducing us to reference [72]. Many thanks are also due to Stefan Müller (MPI, Leipzig) for valuable suggestions and for showing us the hierarchical matrix methods. We would like also to thank G. Allaire, F. Murat, and S. R. S. Varadhan for stimulating discussions at the CIRM workshop on random homogenization and P. Schröder for stimulating discussions on spline-based methods. We also thank an anonymous referee for detailed comments and suggestions.

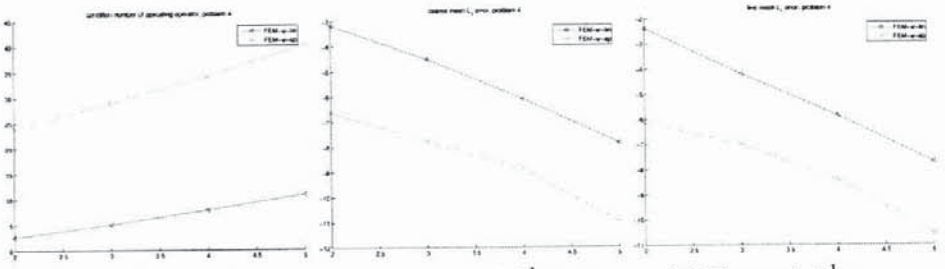

(a) Condition number. (b) Coarse mesh L^1 error. (c) Fine mesh L^1 error.

FIGURE 3.14. Example 3, random Fourier modes.

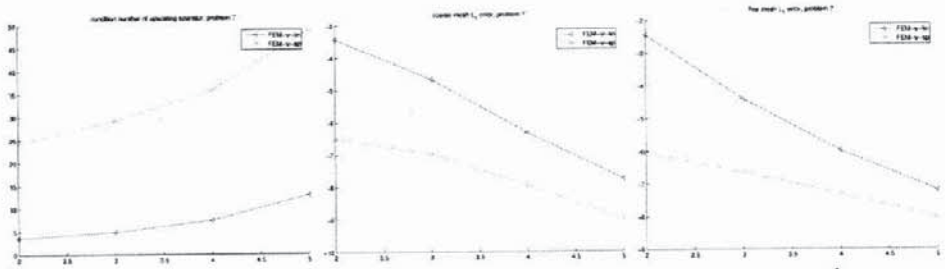

(a) Condition number. (b) Coarse mesh L^1 error. (c) Fine mesh L^1 error.

FIGURE 3.15. Example 5, percolation at criticality.

Coarse mesh error	FEM_ψ_{lin}	FEM_ψ_{sp}
L^1	0.0437	0.0046
L^2	0.0426	0.0052
L^∞	0.0614	0.0096
H^1	0.0746	0.0227

TABLE 3.13. Example 3, random Fourier modes, coarse mesh error.

Fine mesh error	FEM_ψ_{lin}	FEM_ψ_{sp}
L^1	0.0546	0.0077
L^2	0.0529	0.0096
L^∞	0.0920	0.0289
H^1	0.2109	0.0547

TABLE 3.14. Example 3, random Fourier modes, fine mesh error.

Coarse mesh error	FEM_ψ_{lin}	FEM_ψ_{sp}
L^1	0.0393	0.0080
L^2	0.0379	0.0098
L^∞	0.0622	0.0309
H^1	0.0731	0.0404

TABLE 3.15. Example 5, percolation, coarse mesh error.

Fine mesh error	FEM_ψ_{lin}	FEM_ψ_{sp}
L^1	0.0470	0.0099
L^2	0.0464	0.0130
L^∞	0.1174	0.0554
H^1	0.2030	0.0838

TABLE 3.16. Example 5, percolation, fine mesh error.

Bibliography

[1] Alessandrini, G.; Nesi, V. Univalent σ-harmonic mappings: connections with quasiconformal mappings. *J. Anal. Math.* **90** (2003), 197–215.

[2] Allaire, G.; Brizzi, R. A multiscale finite element method for numerical homogenization. Technical report, Le Centre de Mathématiques Appliquées de l'École Polytechnique, Palaiseau, France, 2004.

[3] Alpert, B.; Beylkin, G.; Coifman, R.; Rokhlin, V. Wavelet-like bases for the fast solution of second-kind integral equations. *SIAM J. Sci. Comput.* **14** (1993), no. 1, 159–184.

[4] Ancona, A. Some results and examples about the behavior of harmonic functions and Green's functions with respect to second order elliptic operators. *Nagoya Math. J.* **165** (2002), 123–158.

[5] Armaou, A.; Siettos, C. I.; Kevrekidis, I. G. Time-steppers and 'coarse' control of distributed microscopic processes. Control of complex process systems. *Internat. J. Robust Nonlinear Control* **14** (2004), no. 2, 89–111.

[6] Astala, K.; Nesi, V. Composites and quasiconformal mappings: new optimal bounds in two dimensions. *Calc. Var. Partial Differential Equations* **18** (2003), no. 4, 335–355.

[7] Averbuch, A.; Beylkin, G.; Coifman, R.; Israeli, M. Multiscale inversion of elliptic operators. *Signal and image representation in combined spaces,* 341–359. Wavelet Analysis and Its Applications, 7. Academic Press, San Diego, 1998.

[8] Barlow, M. T.; Coulhon, T.; Kumagai, T. Characterization of sub-Gaussian heat kernel estimates on strongly recurrent graphs. *Comm. Pure Appl. Math.* **58** (2005), no. 12, 1642–1677.

[9] Bebendorf, M. Approximate inverse preconditioning of FE systems for elliptic operators with non-smooth coefficients. Preprint 7/2004, Max-Planck-Institut MiS, Leipzig, 2005.

[10] Bebendorf, M. Efficient inversion of the Galerkin matrix of general second-order elliptic operators with nonsmooth coefficients. *Math. Comp.* **74** (2005), no. 251, 1179–1199.

[11] Bebendorf, M. Why approximate LU decompositions of finite element discretizations of elliptic operators can be computed with almost linear complexity. Preprint 8/2005, Max-Planck-Institut MiS, Leipzig, 2005.

[12] Bebendorf, M.; Chen, Y. Efficient solution of nonlinear elliptic problems using hierarchical matrices with broyden updates. Preprint 51/2005, Max-Planck-Institut MiS, Leipzig, 2005.

[13] Bebendorf, M.; Hackbusch, W. Existence of H-matrix approximants to the inverse FE-matrix of elliptic operators with L^∞-coefficients. *Numer. Math.* **95** (2003), no. 1, 1–28.

[14] Ben Arous, G.; Owhadi, H. Multiscale homogenization with bounded ratios and anomalous slow diffusion. *Comm. Pure Appl. Math.* **56** (2003), no. 1, 80–113.

[15] Bensoussan, A.; Lions, J.-L.; Papanicolaou, G. *Asymptotic analysis for periodic structures.* Studies in Mathematics and Its Applications, 5. North-Holland, Amsterdam-New York, 1978.

[16] Beylkin, G.; Coifman, R.; Rokhlin, V. Fast wavelet transforms and numerical algorithms. I. *Comm. Pure Appl. Math.* **44** (1991), no. 2, 141–183.

[17] Beylkin, G.; Coifman, R.; Rokhlin, V. Fast wavelet transforms and numerical algorithms. I. *Wavelets and applications (Marseille, 1989),* 368–393. RMA: Research Notes in Applied Mathematics, 20. Masson, Paris, 1992.

[18] Beylkin, G.; Coult, N. A multiresolution strategy for reduction of elliptic PDEs and eigenvalue problems. *Appl. Comput. Harmon. Anal.* **5** (1998), no. 2, 129–155.

[19] Brewster, M. E.; Beylkin, G. A multiresolution strategy for numerical homogenization. *Appl. Comput. Harmon. Anal.* **2** (1995), no. 4, 327–349.

[20] Brezzi, F.; Marini, D. Subgrid phenomena and numerical schemes. *Frontiers in numerical analysis (Durham, 2002),* 1–16. Universitext, Springer, Berlin, 2003.

[21] Briane, M.; Milton, G. W.; Nesi, V. Change of sign of the corrector's determinant for homogenization in three-dimensional conductivity. *Arch. Ration. Mech. Anal.* **173** (2004), no. 1, 133–150.

[22] Campanato, S. Un risultato relativo ad equazioni ellittiche del secondo ordine di tipo non variazionale. *Ann. Scuola Norm. Sup. Pisa (3)* **21** (1967), 701–707.

[23] Chertock, A.; Levy, D. On wavelet-based numerical homogenization. *Multiscale Model. Simul.* **3** (2004/05), no. 1, 65–88.

[24] Cirak, F.; Ortiz, M.; Schröder, P. Subdivision surfaces: a new paradigm for thin-shell finite-element analysis. *Internat. J. Numer. Methods Engrg.* **47** (2000), no. 12, 2039–2072.

[25] Clothilde, M. Sur les singularités oscillantes et les formalsime multifractal. Doctoral dissertation, University of Paris XII, 2002.

[26] Coifman, R.; Lions, P.-L.; Meyer, Y.; Semmes, S. Compensated compactness and Hardy spaces. *J. Math. Pures Appl. (9)* **72** (1993), no. 3, 247–286.

[27] De Giorgi, E. Sulla differenziabilità e l'analiticità delle estremali degli integrali multipli regolari. *Mem. Accad. Sci. Torino. Cl. Sci. Fis. Mat. Nat. (3)* **3** (1957), 25–43.

[28] Dolbow, J.; Khaleel, M. A.; Mitchell, J. Multiscale mathematics initiative: a roadmap. Report from the 3rd DOE workshop on multiscale mathematics. Technical report, Department of Energy, Washington, D.C., December 2004. Available at:
`http://www.sc.doe.gov/ascr/mics/amr`

[29] Dorobantu, M.; Engquist, B. Wavelet-based numerical homogenization. *SIAM J. Numer. Anal.* **35** (1998), no. 2, 540–559.

[30] E, W.; Engquist, B.; Li, X.; Ren, W.; Vanden-Eijnden, E. The heterogeneous multiscale method: a review. Technical report, preprint, 2005. Available at:
`http://www.math.princeton.edu/multiscale/review.pdf`

[31] Efendiev, Y. R.; Hou, T. Y.; Wu, X.-H. Convergence of a nonconforming multiscale finite element method. *SIAM J. Numer. Anal.* **37** (2000), no. 3, 888–910.

[32] Ellis, R. S. *Entropy, large deviations, and statistical mechanics.* Grundlehren der Mathematischen Wissenschaften, 271. Springer, New York, 1985.

[33] Ern, A.; Guermond, J.-L. *Theory and practice of finite elements.* Applied Mathematical Sciences, 159. Springer, New York, 2004.

[34] Farhat, C.; Harari, I.; Franca, L. P. The discontinuous enrichment method. *Comput. Methods Appl. Mech. Engrg.* **190** (2001), no. 48, 6455–6479.

[35] Farhat, C.; Harari, I.; Hetmaniuk, U. The discontinuous enrichment method for multiscale analysis. Multiscale computational mechanics for materials and structures (Cachan, 2002). *Comput. Methods Appl. Mech. Engrg.* **192** (2003), no. 28-30, 3195–3209.

[36] Fenn, M.; Steidl, G. *Fmm and $\mathcal{H}$-matrices: a short introduction to the basic idea.* Technical report. TR-2002-008, Department for Mathematics and Computer Science, University of Mannheim, 2004. Available at: `http://bibserv7.bib.uni-mannheim.de/madoc/volltexte/2004/744/pdf/TR=02=008.pdf`

[37] Fish, J.; Wagiman, A. Multiscale finite element method for a locally nonperiodic heterogeneous medium. *Comput. Mech.* **12** (1993), no. 3, 164–180.

[38] Fish, J.; Yuan, Z. Multiscale enrichment based on the partition of unity. *Internat. J. Numer. Methods Engrg.* **62** (2005), no. 10, 1341–1359.

[39] Freiberg, U.; Zähle, M. Harmonic calculus on fractals—a measure geometric approach. I. *Potential Anal.* **16** (2002), no. 3, 265–277.

[40] Freiberg, U. Analytical properties of measure geometric Krein-Feller-operators on the real line. *Math. Nachr.* **260** (2003), 34–47.

[41] Frisch, U.; Parisi, G. Fully developed turbulence and intermittency. *Proceedings of the International Summer School on Turbulence and Predictability in Geophysical Fluid Dynamics and Climate Dynamics,* 84–88. North Holland, Amsterdam, 1985.

[42] Gilbert, A. C. A comparison of multiresolution and classical one-dimensional homogenization schemes. *Appl. Comput. Harmon. Anal.* **5** (1998), no. 1, 1–35.

[43] Goubet, O. Séparation des variables dans le problème de Stokes. Application à son approximation multiéchelles éléments finis. *C. R. Acad. Sci. Paris Sér. I Math.* **315** (1992), no. 12, 1315–1318.

[44] Greengard, L.; Rokhlin, V. A fast algorithm for particle simulations. *J. Comput. Phys.* **73** (1987), no. 2, 325–348.

[45] Hackbusch, W. On the multigrid method applied to difference equations. *Computing* **20** (1978), no. 4, 291–306.

[46] Hackbusch, W.; Grasedyck, L.; Börm, S. An introduction to hierarchical matrices. Proceedings of EQUADIFF, 10 (Prague, 2001). *Math. Bohem.* **127** (2002), no. 2, 229–241.

[47] Hoang, V. H.; Schwab, C. High-dimensional finite elements for elliptic problems with multiple scales. *Multiscale Model. Simul.* **3** (2004/05), no. 1, 168–194.

[48] Höllig, K. *Finite element methods with B-splines.* Frontiers in Applied Mathematics, 26. Society for Industrial and Applied Mathematics (SIAM), Philadelphia, 2003.

[49] Höllig, K.; Reif, U.; Wipper, J. Weighted extended B-spline approximation of Dirichlet problems. *SIAM J. Numer. Anal.* **39** (2001), no. 2, 442–462.

[50] Hou, T. Y.; Wu, X.-H. A multiscale finite element method for elliptic problems in composite materials and porous media. *J. Comput. Phys.* **134** (1997), no. 1, 169–189.

[51] Hou, T. Y.; Wu, X.-H.; Zhang, Y. Removing the cell resonance error in the multiscale finite element method via a Petrov-Galerkin formulation. *Commun. Math. Sci.* **2** (2004), no. 2, 185–205.

[52] Jaffard, S. Formalisme multifractal pour les fonctions. *C. R. Acad. Sci. Paris Sér. I Math.* **317** (1993), no. 8, 745–750.

[53] Jenny, P.; Lee, S. H.; Tchelepi, H. A. Multi-scale finite-volume method for elliptic problems in subsurface flow simulation. *J. Comput. Phys.* **187** (2003), 47–67.

[54] Jikov, V. V.; Kozlov, S. M.; Oleĭnik, O. A. *Homogenization of differential operators and integral functionals.* Springer, Berlin, 1994.

[55] Kigami, J. Harmonic calculus on limits of networks and its application to dendrites. *J. Funct. Anal.* **128** (1995), no. 1, 48–86.

[56] Leonardi, S. Weighted Miranda-Talenti inequality and applications to equations with discontinuous coefficients. *Comment. Math. Univ. Carolin.* **43** (2002), no. 1, 43–59.

[57] Maugeri, A.; Palagachev, D. K.; Softova, L. G. *Elliptic and parabolic equations with discontinuous coefficients*. Mathematical Research, 109. Wiley-VCH, Berlin, 2000.

[58] Meyer, M.; Desbrun, M.; Schröder, P.; Barr, A. H. Discrete differential-geometry operators for triangulated 2-manifolds. *Visualization and mathematics III*, 35–57. Mathematics and Visualization. Springer, Berlin, 2003.

[59] Moser, J. On Harnack's theorem for elliptic differential equations. *Comm. Pure Appl. Math.* **14** (1961), 577–591.

[60] Murat, F. Compacité par compensation. *Ann. Scuola Norm. Sup. Pisa Cl. Sci. (4)* **5** (1978), no. 3, 489–507.

[61] Murat, F.; Tartar, L. H-convergence. *Topics in the mathematical modelling of composite materials*, 21–43. Progress in Nonlinear Differential Equations and Their Applications, 31. Birkhäuser, Boston, 1997.

[62] Nadler, B.; Lafon, S.; Coifman, R. R.; Kevrekidis, I. G. Diffusion maps, spectral clustering and reaction coordinates of dynamical systems. arXiv: math.NA/0503445, 2005.

[63] Nash, J. Continuity of solutions of parabolic and elliptic equations. *Amer. J. Math.* **80** (1958), 931–954.

[64] Oberai, A. A.; Pinsky, P. M. A multiscale finite element method for the Helmholtz equation. *Comput. Methods Appl. Mech. Engrg.* **154** (1998), no. 3-4, 281–297.

[65] Owhadi, H. Anomalous slow diffusion from perpetual homogenization. *Ann. Probab.* **31** (2003), no. 4, 1935–1969.

[66] Owhadi, H. Averaging versus chaos in turbulent transport? *Comm. Math. Phys.* **247** (2004), no. 3, 553–599.

[67] Owhadi, H.; Zhang, L. Homogenization of parabolic equations with a continuum of space and time scales. Preprint, 2005.

[68] Riedi, R. H. An introduction to multifractals. Technical report, Rice University, 1997. Available at: `http://www.stat.rice.edu/~riedi/`.

[69] Shenoy, V. B.; Miller, R.; Tadmor, E. B.; Rodney, D.; Phillips, R.; Ortiz, M. An adaptive finite element approach to atomic-scale mechanics—the quasicontinuum method. *J. Mech. Phys. Solids* **47** (1999), no. 3, 611–642.

[70] Simon, L. Global estimates of Hölder continuity for a class of divergence-form elliptic equations. *Arch. Rational Mech. Anal.* **56** (1974), 253–272.

[71] Strichartz, R. S. Function spaces on fractals. *J. Funct. Anal.* **198** (2003), no. 1, 43–83.

[72] Stroock, D. W.; Zheng, W. Markov chain approximations to symmetric diffusions. *Ann. Inst. H. Poincarè Probab. Statist.* **33** (1997), no. 5, 619–649.

[73] Tartar, L. Compensated compactness and applications to partial differential equations. *Nonlinear analysis and mechanics: Heriot-Watt Symposium, Vol. IV*, 136–212. Research Notes in Mathematics, 39. Pitman, Boston-London, 1979.

[74] Tartar, L. Homogénéisation et compacité par compensation. *Séminaire Goulaouic-Schwartz (1978/1979)*, Exp. No. 9, 9 pp. École Polytechnique, Palaiseau, France, 1979.

[75] Wan, W. L.; Chan, T. F.; Smith, B. An energy-minimizing interpolation for robust multigrid methods. *SIAM J. Sci. Comput.* **21** (1999/2000), no. 4, 1632–1649.

[76] Xu, J. An introduction to multigrid convergence theory. *Iterative methods in scientific computing (Hong Kong, 1995)*, 169–241. Springer, Singapore, 1997.

[77] Xu, J.; Qin, J. Some remarks on a multigrid preconditioner. *SIAM J. Sci. Comput.* **15** (1994), no. 1, 172–184.

[78] Zinsmeister, M. *Thermodynamic formalism and holomorphic dynamical systems.* SMF/AMS Texts and Monographs, 2. American Mathematical Society, Providence, R.I.; Société Mathématique de France, Paris, 2000.

HOUMAN OWHADI
California Institute of Technology
Department of Applied
and Computational Mathematics
1200 E. California Boulevard
MC 217-50
Pasadena, CA 91125
E-mail: owhadi@caltech.edu

LEI ZHANG
California Institute of Technology
Department of Applied
and Computational Mathematics
1200 E. California Boulevard
MC 217-50
Pasadena, CA 91125
E-mail: zhanglei@
acm.caltech.edu

Received May 2005.
Revised September 2005.